EUROPEAN JOURNAL OF PURE AND APPLIED MATHEMATICS
2026, Vol. 19, Issue 3, Article Number 7378
ISSN 1307-5543 – ejpam.com
Published by New York Business Global

Rank-Preserving Encryption for Cotangent Similarity Using Complex Neutrosophic Sets

Maha Alammari[1], Arif Mehmood[2,*]

[1] *Department of Mathematics College of Science King Saud University P.O. Box 22452 Riyadh 11495 Saudi Arabia.*
[2] *Department of Mathematics, Institute of Numerical Sciences, Gomal University, Dera Ismail Khan 29050, KPK, Pakistan.*

Abstract. We present a privacy-preserving pipeline for pairwise comparison of complex neutrosophic sets (CNS) that uses a rank-preserving (order-preserving) encryption to pairwise compare cotangent similarity (CotSM). We introduce a visual analysis method for paired target source relationships using rank-preserving encryption that maintains anonymity. On a 3x3 grid of targets (T_1-T_3) and sources (S_1-S_3), we produce complementary views: (i) Cotangent Similarity (CotSM) Heatmaps and bar charts, all of which are encrypted; and (ii) Pearson-correlation Heatmaps and 3D surfaces, which are likewise encrypted. T_1-S_2 (i.e., max 0.4324 in Heatmaps; 0.6653 in bars) relationship is consistently the most significant in all CotSM perspectives, with T_1 typically dominating and S_2 the most convincing source. On the other hand, encrypted Pearson views had the highest T_3 S_3 value (normalized maximum 1.000), with T_3 dominating and S_3 having the biggest influence. The following is a summary of these findings: (1) Since the encryption maintains rank structure (maxima, minima, relative ranking), comparative interpretation is preserved even while veiled magnitudes in T_1-S_2 are encouraged; and (2) metric selection alters T_3-S_3 receives a high rank from Pearson's emphasis on linear alignment, whereas T_1-S_2 receives a high rank from COTSM's emphasis on similarity geometry. These hierarchies are only scaled or reformulated by normalization (01) and 3D surfaces. The final result is a secure, understandable pipeline that permits signal matching templates, model selection, and pattern recognition without revealing raw data. Strict data confidentiality is necessary, however this can be used directly in any scenario where any sensitive bi-paired connection needs to be examined, such as biological indications, user item affinities, or multi-sensors fusions.

2020 Mathematics Subject Classifications: 03E72, 94A60, 68T37, 90B50

Key Words and Phrases: Neutrosophic Set (NS), single-Valued Neutrosophic Set (SVNS), complex Single-Valued Neutrosophic Set (CSVNS), rank-Preserving Encryption, cotangent Similarity Measure (CotSM).

1. Introduction

The improvement of intelligent systems employed in decision-making, particularly in complicated and uncertain environments, has been greatly aided by the development of fuzzy set and logic theories. Fuzzy set theory was initially applied in this field to develop sophisticated reasoning systems, such as the case-based reasoning method for medical diagnosis put forward by [1]. This article demonstrated the value of fuzzy sets in handling the ambiguity and imprecision of real-world diagnostic procedures. The following generation of researchers used the concept of neutrosophic sets to model over a wider spectrum of uncertainty. Indicatively, [2] has been able to use single-valued neutrosophic sets to medical diagnostics with a superior ability to manage truth-membership and false-membership as well as indeterminacy. Uncertainty-based sets are

*Corresponding Author.
DOI: https://doi.org/10.29020/nybg.ejpam.v19i3.7378

Email addresses: (malammari@ksu.edu.sa) (M. Alammari), (mehdaniyal@gmail.com) (A. Mehmood)

helpful in other aspects of life, such as image processing, in addition to decision-making. [3] demonstrated the importance of this type of theory in feature extraction and pattern recognition by using fuzzy sets that performed well in image segmentation based on histogram thresholding. The seminal work Intuitionistic Fuzzy Sets (IFS) by [4] provided a more critical extension of fuzzy set theory and a more intricate framework for describing uncertainty by introducing a natural degree of non-membership.

This expansion of set theories in an attempt to more fully reflect reality on the ground gave rise to the earliest idea of neutrosophy, which was proposed by [5] and explicitly accepts truth, false, and indeterminacy as independent concepts. Neutrosophy: According to [6], neutrosophic probability, set, and logic are a common language in logics. The neutrosophic structure was then improved into a more useful form that was used in computational and decision-making models by Single-Valued Neutrosophic Sets (SVNS) defined by [7] and Interval Neutrosophic Sets (INS) defined by [8]. This was improved by later studies, such as [9] on simplified neutrosophic sets, which made these concepts ever more comprehensible and helpful in multi-criteria group decision-making (MCGDM) scenarios. The theoretical landscape was also enhanced by the definition of several extensions, such as the neutrosophic soft set [10], which added the property of parameterization of soft sets, and the complex neutrosophic set [11], which added the use of two-dimensional, complex-valued membership grades to deal with periodic and phase-based uncertainty. Their degree of information synthesis in these intricate sets of situations has been made possible by the creation of specialized aggregation operators.

Indeed, [12] extended the TOPSIS approach to apply it to single-valued neutrosophic linguistic numbers, and [13] developed a simpler neutrosophic linguistic normalized weighted Bonferonni mean operator to characterize the relationship between features. In more complicated situations, like the TODIM technique applied to multi-valued neutrosophic sets to provide a more sophisticated situation of decision making [14], the neutrosophic framework proved to be useful and adaptable. Meanwhile, the conceptual scope of neutrosophy was extended by hybrid constructs like rough neutrosophic sets [15], neutrosophic cubic sets [16], and their variations by complex fuzzy sets [17], which are intended to handle a particular kind of hybrid uncertainty and data relations. The mathematical principles of these aggregation processes frequently use classical aggregation operators like the Bonferonni mean [18], which were improved in the fuzzy and uncertain literature through the power average operator [19] and the prioritized aggregation operators [20], to reduce the impact of the largest and most extreme values and the preference levels, respectively. A common basis for producing a range of aggregating functions is also provided by another generic category of fuzzy operators [21]. The theoretical contributions are visible in many facets of decision-making and are very helpful in practice. To demonstrate this, [22] used WASPAS with single-valued neutrosophic sets to identify sustainable sites, while [23] used SVNS and the Fuzzy Delphi Method to analyze customer motivations.

Several neutrosophic improvements to the popular TOPSIS method have been proposed, such as a model that uses the WIFI network as its input [24], an expanded version with an integrated weight measure [25], and a model based on non-linear programming [26]. Additional applications for neutrosophic sets include uncertainty assessment in project time-cost tradeoffs [27], a new plithogenic model of sustainable supply chain risk management [28], and resource leveling issues in construction with a neutrosophic environment [29]. It has also been used to more complicated settings, as simpler neutrosophic hesitant fuzzy environments [30], and bipolar neutrosophic information to new decision-making approaches [31]. Outside of management science, the paradigm has proven useful in statistical analysis, such as the neutrosophic analysis of variance [32], and even in mathematics, where it has produced new methods for solving differential equations with trapezoid neutrosophic numbers [33]. In the neutrosophic field, the development and use of similarity metrics has been an important and vast field of research.

1.1. Literature Review

Early research by [34] introduced many of the first similarity metrics of neutrosophic sets, which led to the creation of numerous other methods. A related study by [35] looked at the application of correlation coefficient in multi-criteria decision-making (MCDM) within a single-valued neutrosophic environment, whereas [36] and [37] addressed the issue of aggregation operator and similarity measures of vectors in simplified neutrosophic sets, respectively. Distance-based similarity measures are used in [38] to cluster single-valued neutrosophic sets. These metrics are used to practical problems, such medical diagnostics, where [39] created single-valued neutrosophic clustering algorithms and [40] enhanced cosine similarity metrics. Additional measurements on more general MCDM applications [41] and similarity measurements on fault identification using the cotangent function [42] were made possible by further algorithmic developments. Apart from examining the basic properties of neutrosophic sets, [43] looked into the ideas of similarity and entropy, and [44] suggested a neutrosophic tangent measure of similarity. The usefulness of these metrics in healthcare remained an area of research since [45] used a tangent-based similarity to multi-period medical diagnosis. During this time, distance-based methods were also developed, including the weighted distance measure of group decision-making [46], a novel distance measure of SVNSs [47], and an enhanced similarity measure for determining minimal spanning trees [48].
The new types of measures included bi-parametric distance measures [49], hybrid vector similarity measures [50], and centroid-based similarity measurements to pattern recognition [51]. Additionally, in 2017 [52], simplified neutrosophic exponential similarity metrics were established for assessing medical symptoms. Additionally presented were the entropy, cross-entropy, and similarity measure of single-valued neutrosophic sets and its use in multi-attribute decision making [53].The study of entropy, similarity, and cross-entropy was repeated in research, along with enhanced symmetry measurements, a sine entropy weight model [54], and specialized measures like the hybrid binary logarithm similarity [55] and the hyperbolic sine similarity measure [56]. [57] presented further suggested measures of similarity of simplified neutrosophic sets and their applications, whereas [58] provided measures of similarity based on Euclidean distance to medical diagnosis. Recent developments include a similarity measure based on prospect theory [59], a novel multi-parametric similarity measure to evaluate large data [60], and a similarity measure based on chi-squared distance [61]. Similarity measures were developed as a result of important developments in the study of entropy and correlation in neutrosophic environments. The single-valued neutrosophic entropy of order 2 and the single-valued neutrosophic entropy of order 2 with similarity of order 2 were previously introduced by [62] and [63]. Further entropy studies included extending distance-based entropy and dimension root entropy to simpler neutrosophic sets [64] and entropy measures using the neutrosophic set in multi-criteria decision making [65]. Recent studies have extended complex cubic intuitionistic fuzzy sets to algebraic structures [66] and established complex tangent trigonometric algorithms for advanced fuzzy sets [67]. Additionally, the analysis of minimal units in fuzzy neutrosophic rings [68] and the foundational work on topological spaces using symbolic n-plithogenic intervals [69] show the expanding frontier of this field, offering a solid mathematical foundation for handling problems with inherent ambiguity and multifaceted information. Both soft set theory and the study of supra open soft sets and its many decompositions and applications are superseded by supra soft topology, according to the sources cited. The foundational contributions of El-Sheikh and Abd Ellatif [70] introduced the concept of soft continuity in this context along with basic results on decompositions of supra soft sets. Supra soft strongly generalized closed sets [71], supra soft strongly extra generalized closed sets [72], and supra soft strongly $semi*$ generalized closed sets [73] are the particular classes of soft sets that are presently being studied in this field. Furthermore, the ideas have been crucial in defining and examining different kinds of soft connectedness [74] and related soft separation axioms [75][76][77]. Studies of interactions with soft ideals [78] and supra soft compactness [79] have also benefitted the theory. Floquet engineering can be

used to dynamically regulate topological superconductors, leading to new point-gapped phases [80].Meanwhile, non-Hermitian systems exhibit unique second-order topological phases and the bipolar skin effect, as demonstrated in photonic kagome crystals [81].These developments pave the way for the development of robust and manageable topological states.

1.2. Motivation and Novelty

In essence, decision-makers are interested in whether a certain connection is larger (top-k, winners), but not in its size, hence sensitive target-source relations should be evaluated without disclosing the magnitude. Stake holders also reject black-box privacy; analysis must be verified, and rankings must be verified across perspectives rather than in haphazard descriptions. When Cot SM and Pearson are presented together, methodology is held accountable since the choice of metric can change results; if your conclusions are reversed, you can see it and provide an explanation. The operational utility outweighs full secrecy in rank decisions if the decision is the ultimate outcome: It is appropriate to compromise between exposing order and safeguarding scale.
Reusable and ready for presentation, the artifacts allow for the sharing of encrypted visualizations between institutions or with non-cleared teams without the burden of sharing raw data. Recommender affinities, multi-sensor fusion, and biological signals are all in the same pipeline, which cuts down on redundant tooling and review time. The new rank-preserving visual analytics pipeline may be used to see and verify heatmaps, bar charts, and 3D surfaces. It intentionally use order-preserving encoding to hide magnitudes while keeping the same ranks (argmax/min, top-k). Instead of giving the misleading impression that one metric is the truth, it offers a two-metric audit of the story of the output of the same encrypted matrix comprising CotSM vs. Pearson to show how the choice of metric changes conclusions ($T_1->S_2$ vs. $T_3->S_3$). It demonstrates that it is view-invarient in a re-scaling: stake holders can rely on patterns between plots because min max normalization and 3D re-expression are re-scaling invariant, meaning they do not change hierarchy. Even with encryption, which privacy work rarely shows directly, it produces outputs that are concretely inspectable in the privacy maxima are circled and constant across views. Additionally, it is a drop-in for delicate pairwise tasks (signal template, user item, sensor fusion) where judgments are made based on comparative ranking rather than values.

2. Preliminaries

We will provide some background information for the current study in this part.

Definition 1. *[5, 6] Suppose $\mathbb{U}$ be a discourse universe. The neutrosophic set $\mathbb{P}$ can then be expressed as follows:*

$$\mathbb{P} = \{\langle \dot{\mathbf{x}}, \mathbb{T}_{\mathbb{P}}(\dot{\mathbf{x}}), \mathbb{I}_{\mathbb{P}}(\dot{\mathbf{x}}), \mathbb{F}_{\mathbb{P}}(\dot{\mathbf{x}})\rangle : \dot{\mathbf{x}} \in \mathbb{U}\}$$

where the function $\mathbb{T}$, $\mathbb{I}$, $\mathbb{F} \longrightarrow]^-0,^+1[$ defines, respectively, truth membership, indeterminacy, and False membership of the element $\dot{\mathbf{x}} \in \mathbb{U}$ to the set $\mathbb{P}$ satisfying the following condition.

$$^-0 \leq sup\mathbb{T}_{\mathbb{P}}(\dot{\mathbf{x}}) + sup\mathbb{I}_{\mathbb{P}}(\dot{\mathbf{x}}) + sup\mathbb{F}_{\mathbb{P}}(\dot{\mathbf{x}}) \leq 3^+$$

From a philosophical point of view, the neutrosophic set uses actual standard or non-standard subsets of $]^-0, 1^+[$. Since $]^-0, 1^+[$ will be difficult to employ in practical applications such as scientific and engineering difficulties, the interval $[0, 1]$ must be used for technical applications instead.

Definition 2. *[5, 6] Suppose two neutrosophic sets (NSs),*

$$\mathbb{P}_{NS} = \{\langle \dot{\mathbf{x}}, \mathbb{T}_{\mathbb{P}}(\dot{\mathbf{x}}), \mathbb{I}_{\mathbb{P}}(\dot{\mathbf{x}}), \mathbb{F}_{\mathbb{P}}(\dot{\mathbf{x}})\rangle : \dot{\mathbf{x}} \in \mathbb{X}\}$$

and

$$\mathbb{Q}_{NS} = \{\langle \dot{\mathbf{x}}, \mathbb{T}_Q(\dot{\mathbf{x}}), \mathbb{I}_Q(\dot{\mathbf{x}}), \mathbb{F}_Q(\dot{\mathbf{x}})\rangle : \dot{\mathbf{x}} \in \mathbb{X}\}$$

then $\mathbb{P}_{NS} \subseteq \mathbb{Q}_{NS}$ *if and only if* $\mathbb{T}_{\mathbb{P}}(\dot{\mathbf{x}}) \leq \mathbb{T}_Q(\dot{\mathbf{x}}), \mathbb{I}_{\mathbb{P}}(\dot{\mathbf{x}}) \geq \mathbb{I}_Q(\dot{\mathbf{x}}), \mathbb{F}_{\mathbb{P}}(\dot{\mathbf{x}}) \geq \mathbb{F}_Q(\dot{\mathbf{x}})$.

Definition 3. *[5, 6] Suppose two NSs,*

$$\mathbb{P}_{NS} = \{\langle \dot{\mathbf{x}}, \mathbb{T}_{\mathbb{P}}(\dot{\mathbf{x}}), \mathbb{I}_{\mathbb{P}}(\dot{\mathbf{x}}), \mathbb{F}_{\mathbb{P}}(\dot{\mathbf{x}})\rangle : \dot{\mathbf{x}} \in \mathbb{X}\}$$

and

$$\mathbb{Q}_{NS} = \{\langle \dot{\mathbf{x}}, \mathbb{T}_Q(\dot{\mathbf{x}}), \mathbb{I}_Q(\dot{\mathbf{x}}), \mathbb{F}_Q(\dot{\mathbf{x}})\rangle : \dot{\mathbf{x}} \in \mathbb{X}\}$$

then $\mathbb{P}_{NS} = \mathbb{Q}_{NS}$ *iff* $\mathbb{T}_{\mathbb{P}}(\dot{\mathbf{x}}) = \mathbb{T}_Q(\dot{\mathbf{x}}), \mathbb{I}_{\mathbb{P}}(\dot{\mathbf{x}}) = \mathbb{I}_Q(\dot{\mathbf{x}}), \mathbb{F}_{\mathbb{P}}(\dot{\mathbf{x}}) = \mathbb{F}_Q(\dot{\mathbf{x}})$.

Definition 4. *[7] Suppose* $\mathbb{X}$ *be a space of points (objects), and* $\dot{\mathbf{x}}$ *represent generic elements in* $\mathbb{X}$*. The truth membership function* $\mathbb{T}_{\mathbb{A}}\dot{\mathbf{x}}$*, indeterminacy membership function* $\mathbb{I}_{\mathbb{A}}\dot{\mathbf{x}}$*, and false membership function* $\mathbb{F}_{\mathbb{A}}\dot{\mathbf{x}}$ *define a SVNS* $\mathbb{A}$ *in* $\mathbb{X}$*. Every point* $\dot{\mathbf{x}} \in \mathbb{X}$ *has* $\mathbb{T}_{\mathbb{A}}\dot{\mathbf{x}}, \mathbb{I}_{\mathbb{A}}\dot{\mathbf{x}}, \mathbb{F}_{\mathbb{A}}\dot{\mathbf{x}} \in [0,1]$ *and* $0 \leq \mathbb{T}_{\mathbb{A}}\dot{\mathbf{x}} + \mathbb{I}_{\mathbb{A}}\dot{\mathbf{x}} + \mathbb{F}_{\mathbb{A}}\dot{\mathbf{x}} \leq 3$*. Consequently, an SVNS* $\mathbb{A}$ *can be expressed as*

$$\mathbb{A} = \{\langle \dot{\mathbf{x}}, \mathbb{T}_{\mathbb{A}}\dot{\mathbf{x}}, \mathbb{I}_{\mathbb{A}}\dot{\mathbf{x}}, \mathbb{F}_{\mathbb{A}}\dot{\mathbf{x}}\rangle | \dot{\mathbf{x}} \in \mathbb{X}\}.$$

Definition 5. *[7] Let* $\mathbb{A}$ *be an SVNS over* $\mathbb{X}$*. Next,* $\mathbb{A}^c$ *represents the complement of* $\mathbb{A}$ *and is;*

$$\mathbb{A}^c = \{\langle \dot{\mathbf{x}}, \mathbb{F}_{\mathbb{A}}\dot{\mathbf{x}}, 1 - \mathbb{I}_{\mathbb{A}}\dot{\mathbf{x}}, \mathbb{T}_{\mathbb{A}}\dot{\mathbf{x}}\rangle | \dot{\mathbf{x}} \in \mathbb{X}\}$$

3. Complex Single Valued Neutrosophic Sets

Definition 6. *[82] A truth membership function* $\mathbb{T}_{\mathbb{S}}(\dot{\mathbf{x}})$*, a false membership function* $\mathbb{F}_{\mathbb{S}}(\dot{\mathbf{x}})$*, and an indeterminacy membership function* $\mathbb{I}_{\mathbb{S}}(\dot{\mathbf{x}})$ *defines a CNS* $\mathbb{S}$ *based on a universe of discourse* $\mathbb{X}$ *by assigning CV grades to each* $\dot{\mathbf{x}} \in \mathbb{X}$*. The values* $\mathbb{T}_{\mathbb{S}}(\dot{\mathbf{x}})$*,* $\mathbb{I}_{\mathbb{S}}(\dot{\mathbf{x}})$*,* $\mathbb{F}_{\mathbb{S}}(\dot{\mathbf{x}})$*, and their sum are contained in the unit circle of the complex plane and are given by;*

$$\mathbb{T}_{\mathbb{S}}(\dot{\mathbf{x}}) = p_{\mathbb{S}}(\dot{\mathbf{x}})e^{j\mu_{\mathbb{S}}(\dot{\mathbf{x}})}, \quad \mathbb{I}_{\mathbb{S}}(\dot{\mathbf{x}}) = q_{\mathbb{S}}(\dot{\mathbf{x}})e^{j\nu_{\mathbb{S}}(\dot{\mathbf{x}})}, \quad \mathbb{F}_{\mathbb{S}}(\dot{\mathbf{x}}) = r_{\mathbb{S}}(\dot{\mathbf{x}})e^{j\omega_{\mathbb{S}}(\dot{\mathbf{x}})},$$

where $p_{\mathbb{S}}(\dot{\mathbf{x}}), q_{\mathbb{S}}(\dot{\mathbf{x}}), r_{\mathbb{S}}(\dot{\mathbf{x}}) \in [0,1]$ *and* $\mu_{\mathbb{S}}(\dot{\mathbf{x}}), \nu_{\mathbb{S}}(\dot{\mathbf{x}}), \omega_{\mathbb{S}}(\dot{\mathbf{x}})$ *are real-valued functions such that*

$$0 \leq p_{\mathbb{S}}(\dot{\mathbf{x}}) + q_{\mathbb{S}}(\dot{\mathbf{x}}) + r_{\mathbb{S}}(\dot{\mathbf{x}}) \leq 3.$$

The representation of the CNS $\mathbb{S}$ *is*

$$\mathbb{S} = \{\langle \dot{\mathbf{x}}, \mathbb{T}_{\mathbb{S}}(\dot{\mathbf{x}}), \mathbb{I}_{\mathbb{S}}(\dot{\mathbf{x}}), \mathbb{F}_{\mathbb{S}}(\dot{\mathbf{x}})\rangle : \dot{\mathbf{x}} \in \mathbb{X}\},$$

where

$$\mathbb{T}_{\mathbb{S}} : \mathbb{X} \to \{a_{\mathbb{T}} \in \mathbf{C} : |a_{\mathbb{T}}| \leq 1\}, \quad \mathbb{I}_{\mathbb{S}} : \mathbb{X} \to \{a_{\mathbb{I}} \in \mathbf{C} : |a_{\mathbb{I}}| \leq 1\},$$
$$\mathbb{F}_{\mathbb{S}} : \mathbb{X} \to \{a_{\mathbb{F}} \in \mathbf{C} : |a_{\mathbb{F}}| \leq 1\},$$

and

$$|\mathbb{T}_{\mathbb{S}}(\dot{\mathbf{x}})| + |\mathbb{I}_{\mathbb{S}}(\dot{\mathbf{x}})| + |\mathbb{F}_{\mathbb{S}}(\dot{\mathbf{x}})| \leq 3.$$

In accordance with the original concept of a complex fuzzy set, where the amplitude terms lie in an interval of $(0,1)$ *and the phase terms reside in an interval of* $(0,2\pi]$*, the interval* $(0,2\pi]$ *is selected for the phase term.*

The name "classical neutrosophic set" refers to the situation where these membership functions are real-valued, whereas "CNS" refers to a neutrosophic set with complex-valued truth, indeterminacy, and false membership functions.

Remark 1. *According to the definition given above, ι represents the imaginary number $\iota = \sqrt{-1}$, and it is this imaginary number that gives the CNS its complex-valued membership grades. The exponential form of a complex number is denoted by the expression $e^{\iota\theta}$, which stands for $e^{\iota\theta} = \cos\theta + \iota \sin\theta$.*

Definition 7. *Assume that two CSVNSs exist,*

$$\mathbb{A}_{CSVNS} = \{\langle \dot{\mathbf{x}}, \mathbb{T}_{\mathbb{A}}(\dot{\mathbf{x}}), \mathbb{I}_{\mathbb{A}}(\dot{\mathbf{x}}), \mathbb{F}_{\mathbb{A}}(\dot{\mathbf{x}})\rangle : \dot{\mathbf{x}} \in \mathbb{X}\}$$

and

$$\mathbb{B}_{CSVNS} = \{\langle \dot{\mathbf{x}}, \mathbb{T}_{\mathbb{B}}(\dot{\mathbf{x}}), \mathbb{I}_{\mathbb{B}}(\dot{\mathbf{x}}), \mathbb{F}_{\mathbb{B}}(\dot{\mathbf{x}})\rangle : \dot{\mathbf{x}} \in \mathbb{X}\}$$

then $\mathbb{A}_{CSVNS} \subseteq \mathbb{B}_{CSVNS}$ iff $\mathbb{T}_{\mathbb{A}}(\dot{\mathbf{x}}) \leq \mathbb{T}_{\mathbb{B}}(\dot{\mathbf{x}}), \mathbb{I}_{\mathbb{A}}(\dot{\mathbf{x}}) \geq \mathbb{I}_{\mathbb{B}}(\dot{\mathbf{x}}), \mathbb{F}_{\mathbb{A}}(\dot{\mathbf{x}}) \geq \mathbb{F}_{\mathbb{B}}(\dot{\mathbf{x}})$.

Definition 8. *Assume that two CSVNSs (CSVNSs) exist,*

$$\mathbb{A}_{CSVNS} = \{\langle \dot{\mathbf{x}}, \mathbb{T}_{\mathbb{A}}(\dot{\mathbf{x}}), \mathbb{I}_{\mathbb{A}}(\dot{\mathbf{x}}), \mathbb{F}_{\mathbb{A}}(\dot{\mathbf{x}})\rangle : \dot{\mathbf{x}} \in \mathbb{X}\}$$

and

$$\mathbb{B}_{CSVNS} = \{\langle \dot{\mathbf{x}}, \mathbb{T}_{\mathbb{B}}(\dot{\mathbf{x}}), \mathbb{I}_{\mathbb{B}}(\dot{\mathbf{x}}), \mathbb{F}_{\mathbb{B}}(\dot{\mathbf{x}})\rangle : \dot{\mathbf{x}} \in \mathbb{X}\}$$

then $\mathbb{A}_{CSVNS} = \mathbb{B}_{CSVNS}$ if and only if $\mathbb{T}_{\mathbb{A}}(\dot{\mathbf{x}}) = \mathbb{T}_{\mathbb{B}}(\dot{\mathbf{x}}), \mathbb{I}_{\mathbb{A}}(\dot{\mathbf{x}}) = \mathbb{I}_{\mathbb{B}}(\dot{\mathbf{x}}), \mathbb{F}_{\mathbb{A}}(\dot{\mathbf{x}}) = \mathbb{F}_{\mathbb{B}}(\dot{\mathbf{x}})$.

Definition 9. *Assume that two CSVNSs over the universe set $\mathbb{X}$ are $\mathbb{A}$ and $\mathbb{B}$. Then, $\mathbb{A} \cup \mathbb{B} = \mathbb{C}$, which represents their union, is referred to:*

$$\mathbb{C} = \{\langle \dot{\mathbf{x}}, \mathbb{T}_{\mathbb{C}}\dot{\mathbf{x}}, \mathbb{I}_{\mathbb{C}}\dot{\mathbf{x}}, \mathbb{F}_{\mathbb{C}}\dot{\mathbf{x}}\rangle : \dot{\mathbf{x}} \in \mathbb{X}\},$$

Where

$$\mathbb{T}_{\mathbb{C}}\dot{\mathbf{x}} = \max\{\mathbb{T}_{\mathbb{A}}\dot{\mathbf{x}}, \mathbb{T}_{\mathbb{B}}\dot{\mathbf{x}}\}$$
$$\mathbb{I}_{\mathbb{C}}\dot{\mathbf{x}} = \max\{\mathbb{I}_{\mathbb{A}}\dot{\mathbf{x}}, \mathbb{I}_{\mathbb{B}}\dot{\mathbf{x}}\}$$
$$\mathbb{F}_{\mathbb{C}}\dot{\mathbf{x}} = \min\{\mathbb{F}_{\mathbb{A}}\dot{\mathbf{x}}, \mathbb{F}_{\mathbb{B}}\dot{\mathbf{x}}\}$$

Definition 10. *Assume that two CSVNSs over the universe set $\mathbb{X}$ are $\mathbb{A}$ and $\mathbb{B}$. Then, $\mathbb{A} \cap \mathbb{B} = \mathbb{C}$, which represents their intersection, is defined by:*

$$\mathbb{C} = \{\langle \dot{\mathbf{x}}, \mathbb{T}_{\mathbb{C}}\dot{\mathbf{x}}, \mathbb{I}_{\mathbb{C}}\dot{\mathbf{x}}, \mathbb{F}_{\mathbb{C}}\dot{\mathbf{x}}\rangle : \dot{\mathbf{x}} \in \mathbb{X}\},$$

Where

$$\mathbb{T}_{\mathbb{C}}\dot{\mathbf{x}} = \min\{\mathbb{T}_{\mathbb{A}}\dot{\mathbf{x}}, \mathbb{T}_{\mathbb{B}}\dot{\mathbf{x}}\}$$
$$\mathbb{I}_{\mathbb{C}}\dot{\mathbf{x}} = \min\{\mathbb{I}_{\mathbb{A}}\dot{\mathbf{x}}, \mathbb{I}_{\mathbb{B}}\dot{\mathbf{x}}\}$$
$$\mathbb{F}_{\mathbb{C}}\dot{\mathbf{x}} = \max\{\mathbb{F}_{\mathbb{A}}\dot{\mathbf{x}}, \mathbb{F}_{\mathbb{B}}\dot{\mathbf{x}}\}$$

Definition 11. *Let $\{\mathbb{A}_{\mathbf{i}} : \mathbf{i} \in \mathbf{I}\}$ be a family of CSVNSs over the universe set $\mathbb{X}$. Then,*

$$\bigcup_{\mathbf{i}\in\mathbf{I}} \mathbb{A}_{\mathbf{i}} = \left\{\langle \dot{\mathbf{x}}, \sup_{\mathbf{i}\in\mathbf{I}} \mathbb{T}_{\mathbb{A}_{\mathbf{i}}}\dot{\mathbf{x}}, \sup_{\mathbf{i}\in\mathbf{I}} \mathbb{I}_{\mathbb{A}_{\mathbf{i}}}\dot{\mathbf{x}}, \inf_{\mathbf{i}\in\mathbf{I}} \mathbb{F}_{\mathbb{A}_{\mathbf{i}}}\dot{\mathbf{x}}\rangle : \dot{\mathbf{x}} \in \mathbb{X}\right\}.$$

$$\bigcap_{\mathbf{i}\in\mathbf{I}} \mathbb{A}_{\mathbf{i}} = \left\{\langle \dot{\mathbf{x}}, \inf_{\mathbf{i}\in\mathbf{I}} \mathbb{T}_{\mathbb{A}_{\mathbf{i}}}\dot{\mathbf{x}}, \inf_{\mathbf{i}\in\mathbf{I}} \mathbb{I}_{\mathbb{A}_{\mathbf{i}}}\dot{\mathbf{x}}, \sup_{\mathbf{i}\in\mathbf{I}} \mathbb{F}_{\mathbb{A}_{\mathbf{i}}}()\rangle : \dot{\mathbf{x}} \in \mathbb{X}\right\}.$$

Definition 12. *A null CSVNS is defined as a CSVNS $\mathbb{A}$ over the universe set $\mathbb{X}$ if*

$$\mathbb{T}_{\mathbb{A}}\dot{\mathbf{x}} = 0, \quad \mathbb{I}_{\mathbb{A}}\dot{\mathbf{x}} = 0, \quad \mathbb{F}_{\mathbb{A}}\dot{\mathbf{x}} = 1, \quad \forall\ \dot{\mathbf{x}} \in \mathbb{X}.$$

The symbol for it is $0_{\mathbb{A}}$.

Definition 13. *A absolute CSVNS is a CSVNS $\mathbb{A}$ over the universe set $\mathbb{X}$ if*

$$\mathbb{T}_{\mathbb{A}}\dot{\mathbf{x}} = 1, \quad \mathbb{I}_{\mathbb{A}}\dot{\mathbf{x}} = 1, \quad \mathbb{F}_{\mathbb{A}}\dot{\mathbf{x}} = 0, \quad \forall\ \dot{\mathbf{x}} \in \mathbb{X},$$

Clearly,

$$0^c_{\mathbb{A}} = 1_{\mathbb{A}}, \quad 1^c_{\mathbb{A}} = 0_{\mathbb{A}}.$$

Proposition 1. *Consider three CSVNSs over the universe set $\mathbb{X}$: $\mathbb{A}$, $\mathbb{B}$, and $\mathbb{C}$. Later,*

(i) $\mathbb{A} \cup [\mathbb{B} \cup \mathbb{C}] = [\mathbb{A} \cup \mathbb{B}] \cup \mathbb{C} and$
$\mathbb{A} \cap [\mathbb{B} \cap \mathbb{C}] = [\mathbb{A} \cap \mathbb{B}] \cap \mathbb{C}$*;*

(ii) $\mathbb{A} \cup [\mathbb{B} \cap \mathbb{C}] = [\mathbb{A} \cup \mathbb{B}] \cap [\mathbb{A} \cup \mathbb{C}] and$
$\mathbb{A} \cap [\mathbb{B} \cup \mathbb{C}] = [\mathbb{A} \cap \mathbb{B}] \cup [\mathbb{A} \cap \mathbb{C}]$*;*

(iii) $\mathbb{A} \cup 0_{\mathbb{A}} = \mathbb{A} and \mathbb{A} \cap 0_{\mathbb{A}} = 0_{\mathbb{A}}$*;*

(iv) $\mathbb{A} \cup 1_{\mathbb{A}} = \mathbb{A} and \mathbb{A} \cap 1_{\mathbb{A}} = \mathbb{A}$*;*

Proof. *Obvious.*

Proposition 2. *Assume that two CSVNSs over the universe set $\mathbb{X}$ are $\mathbb{A}$ and $\mathbb{B}$. Next,*

(i) $[\mathbb{A} \cup \mathbb{B}]^c = \mathbb{A}^c \cap \mathbb{B}^c$

(ii) $[\mathbb{A} \cap \mathbb{B}]^c = \mathbb{A}^c \cup \mathbb{B}^c$

Proof. *(i).* $\forall\ \dot{\mathbf{x}} \in \mathbb{X}$,

$$\begin{aligned}
\mathbb{A} \cup \mathbb{B} &= \{\langle \dot{\mathbf{x}}, \max\{\mathbb{T}_{\mathbb{A}}\dot{\mathbf{x}}, \mathbb{T}_{\mathbb{B}}\dot{\mathbf{x}}\}, \max\{\mathbb{I}_{\mathbb{A}}\dot{\mathbf{x}}, \mathbb{I}_{\mathbb{B}}\dot{\mathbf{x}}\},\\
&\quad \min\{\mathbb{F}_{\mathbb{A}}\dot{\mathbf{x}}, \mathbb{F}_{\mathbb{B}}\dot{\mathbf{x}}\}\rangle\}\\
[\mathbb{A} \cup \mathbb{B}]^c &= \{\langle \dot{\mathbf{x}}, \min\{\mathbb{F}_{\mathbb{A}}\dot{\mathbf{x}}, \mathbb{F}_{\mathbb{B}}\dot{\mathbf{x}}\}, 1 - \max\{\mathbb{I}_{\mathbb{A}}\dot{\mathbf{x}}, \mathbb{I}_{\mathbb{B}}\dot{\mathbf{x}}\},\\
&\quad \max\{\mathbb{T}_{\mathbb{A}}\dot{\mathbf{x}}, \mathbb{T}_{\mathbb{B}}\dot{\mathbf{x}}\}\rangle\}
\end{aligned}$$

Now,

$$\begin{aligned}
\mathbb{A}^c &= \{\langle \dot{\mathbf{x}}, \mathbb{F}_{\mathbb{A}}\dot{\mathbf{x}}, 1 - \mathbb{I}_{\mathbb{A}}\dot{\mathbf{x}}, \mathbb{T}_{\mathbb{A}}\dot{\mathbf{x}}\rangle\}\\
\mathbb{B}^c &= \{\langle \dot{\mathbf{x}}, \mathbb{F}_{\mathbb{B}}\dot{\mathbf{x}}, 1 - \mathbb{I}_{\mathbb{B}}\dot{\mathbf{x}}, \mathbb{T}_{\mathbb{B}}\dot{\mathbf{x}}\rangle\}
\end{aligned}$$

Then,

$$\begin{aligned}
\mathbb{A}^c \cap \mathbb{B}^c &= \{\langle \dot{\mathbf{x}}, \min\{\mathbb{F}_{\mathbb{A}}\dot{\mathbf{x}}, \mathbb{F}_{\mathbb{B}}\dot{\mathbf{x}}\}, \min\{1 - \mathbb{I}_{\mathbb{A}}\dot{\mathbf{x}}, 1 - \mathbb{I}_{\mathbb{B}}\dot{\mathbf{x}}\},\\
&\quad \max\{\mathbb{T}_{\mathbb{A}}\dot{\mathbf{x}}, \mathbb{T}_{\mathbb{B}}\dot{\mathbf{x}}\}\rangle\}\\
&= \{\langle \dot{\mathbf{x}}, \min\{\mathbb{F}_{\mathbb{A}}\dot{\mathbf{x}}, \mathbb{F}_{\mathbb{B}}\dot{\mathbf{x}}\}, 1 - \max\{\mathbb{I}_{\mathbb{A}}\dot{\mathbf{x}}, \mathbb{I}_{\mathbb{B}}\dot{\mathbf{x}}\},\\
&\quad \max\{\mathbb{T}_{\mathbb{A}}\dot{\mathbf{x}}, \mathbb{T}_{\mathbb{B}}\dot{\mathbf{x}}\}\rangle\}
\end{aligned}$$

Therefore, $[\mathbb{A} \cup \mathbb{B}]^c = \mathbb{A}^c \cap \mathbb{B}^c$.
(ii). It is acquired in a comparable manner.

Example 1. *In contemporary systems, information can be encoded or encrypted to deal with uncertainty, noise, and distorted truth. An interstitial description of such situations is given by a complicated neutrosophic set, a complex form of degrees of truth, indeterminacy, and false. Let us assume that the discourse universe is supplied by:*

$$\mathbb{X} = \{\dot{\mathbf{x}}_1, \dot{\mathbf{x}}_2, \dot{\mathbf{x}}_3, \dot{\mathbf{x}}_4\}$$

Now let's look at complicated single-valued neutrosophic sets $\mathbb{A}$ *and,* $\mathbb{B}$ *over the universe set* $\mathbb{X}$. *Every member* $\dot{\mathbf{x}}_{\mathbf{i}} \in \mathbb{X}$ *is represented by an encrypted triple of the following kind:*

$$\dot{\mathbf{x}}_{\mathbf{i}} \to \mathbb{T}(\dot{\mathbf{x}}_{\mathbf{i}}), \mathbb{I}(\dot{\mathbf{x}}_{\mathbf{i}}), \mathbb{F}(\dot{\mathbf{x}}_{\mathbf{i}})$$

where the complex-valued truth, indeterminacy, and false memberships are $\mathbb{T}(\dot{\mathbf{x}}_{\mathbf{i}}), mathdsI(\dot{\mathbf{x}}_{\mathbf{i}}), mathdsF(\dot{\mathbf{x}}_{\mathbf{i}})$, *respectively. The sets then look like this:*

$$\mathbb{A} = \begin{bmatrix} (\langle x_1, 0.7e^{\iota\pi(0.6)}, 0.6e^{\iota\pi(0.4)}, 0.4e^{\iota\pi(0.6)}\rangle, \langle x_2, 0.7e^{\iota\pi(0.6)}, 0.6e^{\iota\pi(0.7)}, 0.4e^{\iota\pi(0.5)}\rangle, \\ \langle x_3, 0.4e^{\iota\pi(0.7)}, 0.2e^{\iota\pi(0.4)}, 0.3e^{\iota\pi(0.1)}\rangle, \langle x_4, 0.5e^{\iota\pi(0.6)}, 0.7e^{\iota\pi(0.9)}, 0.4e^{\iota\pi(0.3)}\rangle) \end{bmatrix}$$

$$\mathbb{B} = \begin{bmatrix} (\langle x_1, 0.4e^{\iota\pi(0.5)}, 0.5e^{\iota\pi(0.4)}, 0.7e^{\iota\pi(0.8)}\rangle, \langle x_2, 0.4e^{\iota\pi(0.4)}, 0.5e^{\iota\pi(0.6)}, 0.7e^{\iota\pi(0.6)}\rangle, \\ \langle x_3, 0.2e^{\iota\pi(0.6)}, 0.1e^{\iota\pi(0.1)}, 0.4e^{\iota\pi(0.3)}\rangle, \langle x_4, 0.3e^{\iota\pi(0.4)}, 0.5e^{\iota\pi(0.3)}, 0.6e^{\iota\pi(0.6)}\rangle) \end{bmatrix}$$

The operations of union and intersection are:

$$\mathbb{A} \cup \mathbb{B} = \begin{bmatrix} (\langle x_1, 0.7e^{\iota\pi(0.6)}, 0.6e^{\iota\pi(0.4)}, 0.4e^{\iota\pi(0.6)}\rangle, \langle x_2, 0.7e^{\iota\pi(0.6)}, 0.6e^{\iota\pi(0.7)}, 0.4e^{\iota\pi(0.5)}\rangle, \\ \langle x_3, 0.4e^{\iota\pi(0.7)}, 0.2e^{\iota\pi(0.4)}, 0.3e^{\iota\pi(0.1)}\rangle, \langle x_4, 0.5e^{\iota\pi(0.6)}, 0.7e^{\iota\pi(0.9)}, 0.4e^{\iota\pi(0.3)}\rangle) \end{bmatrix}$$

$$\mathbb{A} \cap \mathbb{B} = \begin{bmatrix} (\langle x_1, 0.4e^{\iota\pi(0.5)}, 0.5e^{\iota\pi(0.4)}, 0.7e^{\iota\pi(0.8)}\rangle, \langle x_2, 0.4e^{\iota\pi(0.4)}, 0.5e^{\iota\pi(0.6)}, 0.7e^{\iota\pi(0.6)}\rangle, \\ \langle x_3, 0.2e^{\iota\pi(0.6)}, 0.1e^{\iota\pi(0.1)}, 0.4e^{\iota\pi(0.3)}\rangle, \langle x_4, 0.3e^{\iota\pi(0.4)}, 0.5e^{\iota\pi(0.3)}, 0.6e^{\iota\pi(0.6)}\rangle) \end{bmatrix}$$

Each of the three complicated value components in this instance functions as an encrypted piece of data that offers graded information on truth, uncertainty, and false. The phase carries additional directional or hidden information, whereas the amplitude measures the strength of each component. Because of this, complicated neutrosophic sets can be used to represent systems involving encryption, signal processing, and the uncertainty of data transmission to the destination.

4. Cotangent Similarity Measures for CSVNSs

The measure converts the total absolute differences between the three membership components of the features into a similarity score using the cotangent function, where smaller differences indicate greater similarity. This method takes a discriminating approach to truth, untruth, and indeterminacy while providing a nuanced and practical evaluation of CSVNSs. It is especially helpful in multi-criteria decision-making, shape identification, medical diagnosis, and risk assessment since it can manage complex uncertainties and offer a normalized, symmetric, and globally averaged measure of similarity across all features. By normalizing the differences by $\frac{\pi}{4}$ and $\frac{\pi}{12}$, a continuous similarity scale is obtained. A global similarity score can be obtained by averaging many features using cotangent similarity, which is symmetric and highlights small discrepancies. A solid and thorough foundation for comparing CSVNSs in uncertain situations is provided by the ability to manage complicated uncertainty.Let $\mathbb{A} = \langle \dot{\mathbf{x}}, \mathbf{T}_{\mathbb{A}}\dot{\mathbf{x}}, \mathbb{I}_{\mathbb{A}}\dot{\mathbf{x}}, \mathbb{F}_{\mathbb{A}}\dot{\mathbf{x}}\rangle$ and

$\mathbb{B} = \langle \dot{\mathbf{x}}, T_{\mathbb{B}}\dot{\mathbf{x}}, \mathbb{I}_{\mathbb{B}}\dot{\mathbf{x}}, \mathbb{F}_{\mathbb{B}}\dot{\mathbf{x}} \rangle$ be two CSVN numbers. The cotangent similarity function, which determines how similar two vectors are based solely on their direction and ignores the influence of their distance from one another, can now be expressed as follows:

$$Cotangent_{CSVNS}(\mathbb{A}, \mathbb{B}) = \frac{1}{n}\sum_{k=1}^{n}\{\cot[\frac{\pi}{4} + \frac{\pi}{12}(|T_{ik} - T_{jk}| + |I_{ik} - I_{jk}| + |F_{ik} - F_{jk}|)]\}$$

Proposition 3. *The following characteristics are satisfied by the defined cotangent similarity measure $Cot_{CSVNS}(\mathbb{A}, \mathbb{B})$ between $\mathbb{A}$ and $\mathbb{B}$:*

(i) $0 \leq Cot_{CSVNS}(\mathbb{A}, \mathbb{B}) \leq 1$.

(ii) $Cot_{CSVNS}(\mathbb{A}, \mathbb{B}) = 1$ *if and only if* $\mathbb{A} = \mathbb{B}$.

(iii) $Cot_{CSVNS}(\mathbb{A}, \mathbb{B}) = Cot_{CNRS}(\mathbb{B}, \mathbb{A})$.

(iv) *If R is a CSVNS in $\mathbb{X}$ and $\mathbb{A} \subset \mathbb{B} \subset \mathbb{C}$ then $Cot_{CSVNS}(\mathbb{A}, \mathbb{C}) \leq Cot_{CSVNS}(\mathbb{A}, \mathbb{B})$ and $Cot_{CSVNS}(\mathbb{A}, \mathbb{C}) \leq Cot_{CSVNS}(\mathbb{B}, \mathbb{C})$.*

Proof.

(i) Since the value of the cotangent function and the membership, indeterminacy, and non-membership functions of the CSVNSs are all within $[0, 1]$, the cotangent function-based similarity measure is likewise inside $[0, 1]$. Therefore, $0 \leq Cot_{CSVNS}(\mathbb{A}, \mathbb{B}) \leq 1$.

(ii) If $\mathbb{A} = \mathbb{B}$ for any two CSVNS $\mathbb{A}$ and $\mathbb{B}$, then $T_{\mathbb{A}}\dot{\mathbf{x}} = T_{\mathbb{B}}\dot{\mathbf{x}}, I_{\mathbb{A}}\dot{\mathbf{x}} = I_{\mathbb{B}}\dot{\mathbf{x}}, F_{\mathbb{A}}\dot{\mathbf{x}} = F_{\mathbb{B}}\dot{\mathbf{x}}$. Hence $|T_{\mathbb{A}}\dot{\mathbf{x}} - T_{\mathbb{B}}\dot{\mathbf{x}}| = 0$,$|I_{\mathbb{A}}\dot{\mathbf{x}} - I_{\mathbb{B}}\dot{\mathbf{x}}| = 0$, $|F_{\mathbb{A}}\dot{\mathbf{x}} - F_{\mathbb{B}}\dot{\mathbf{x}}| = 0$. Thus $Cot_{CSVNS}(\mathbb{A}, \mathbb{B}) = 1$.
Conversely, If $Cot_{CSVNS}(\mathbb{A}, \mathbb{B}) = 1$ then $|T_{\mathbb{A}}\dot{\mathbf{x}} - T_{\mathbb{B}}\dot{\mathbf{x}}| = 0$,$|I_{\mathbb{A}}\dot{\mathbf{x}} - I_{\mathbb{B}}\dot{\mathbf{x}}| = 0$, $|F_{\mathbb{A}}\dot{\mathbf{x}} - F_{\mathbb{B}}\dot{\mathbf{x}}| = 0$ since $\tan(0) = 0$.
So we can we can write, $T_{\mathbb{A}}\dot{\mathbf{x}} = T_{\mathbb{B}}\dot{\mathbf{x}}, I_{\mathbb{A}}\dot{\mathbf{x}} = I_{\mathbb{B}}\dot{\mathbf{x}}, F_{\mathbb{A}}\dot{\mathbf{x}} = F_{\mathbb{B}}\dot{\mathbf{x}}$. Hence $\mathbb{A} = \mathbb{B}$.

(iii) This is a clear proof.

(iv) If $\mathbb{A} \subset \mathbb{B} \subset \mathbb{C}$ then $T_{\mathbb{A}}\dot{\mathbf{x}} \leq T_{\mathbb{B}}\dot{\mathbf{x}} \leq T_R\dot{\mathbf{x}}$, $I_{\mathbb{A}}\dot{\mathbf{x}} \geq I_{\mathbb{B}}\dot{\mathbf{x}} \geq I_R\dot{\mathbf{x}}$, and $F_{\mathbb{A}}\dot{\mathbf{x}} \geq F_{\mathbb{B}}\dot{\mathbf{x}} \geq F_R\dot{\mathbf{x}}$ for $\dot{\mathbf{x}} \in \mathbb{X}$. The following inequalities are now present:
$|T_{\mathbb{A}}\dot{\mathbf{x}} - T_{\mathbb{B}}\dot{\mathbf{x}}| \leq |T_{\mathbb{A}}\dot{\mathbf{x}} - T_R\dot{\mathbf{x}}|$, $|T_{\mathbb{B}}\dot{\mathbf{x}} - T_R\dot{\mathbf{x}}| \leq |T_{\mathbb{A}}\dot{\mathbf{x}} - T_R\dot{\mathbf{x}}|$;
$|I_{\mathbb{A}}\dot{\mathbf{x}} - I_{\mathbb{B}}\dot{\mathbf{x}}| \leq |I_{\mathbb{A}}\dot{\mathbf{x}} - T_R\dot{\mathbf{x}}|$, $|I_{\mathbb{B}}\dot{\mathbf{x}} - I_R\dot{\mathbf{x}}| \leq |I_{\mathbb{A}}\dot{\mathbf{x}} - I_R\dot{\mathbf{x}}|$;
$|F_{\mathbb{A}}\dot{\mathbf{x}} - F_{\mathbb{B}}\dot{\mathbf{x}}| \leq |F_{\mathbb{A}}\dot{\mathbf{x}} - F_R\dot{\mathbf{x}}|$, $|F_{\mathbb{B}}\dot{\mathbf{x}} - F_R\dot{\mathbf{x}}| \leq |F_{\mathbb{A}}\dot{\mathbf{x}} - F_R\dot{\mathbf{x}}|$;
Thus $Cot_{CSVNS}(\mathbb{A}, \mathbb{C}) \leq Cot_{CSVNS}(\mathbb{A}, \mathbb{B})$ and $Cot_{CSVNS}(\mathbb{A}, \mathbb{C}) \leq Cot_{CSVNS}(\mathbb{B}, \mathbb{C})$. Within the interval $[\frac{\pi}{4}, \frac{\pi}{2}]$, the cotangent function decreases.

4.1. Cotangent Similarity Measure

[83] Suppose $T_i = (\mathbb{T}_{ik}, \mathbb{I}_{ik}, \mathbb{F}_{ik})$, $C_j = (\mathbb{T}_{jk}, \mathbb{I}_{jk}, \mathbb{F}_{jk})$ are two CSVNSs. Then for T_i:
$\mathbb{T}_{ik}$: True membership degree of $kforT_i$.
$\mathbb{I}_{ik}$: Indeterminacy membership degree of $kforT_i$.
$\mathbb{F}_{ik}$: False membership degree of $kforT_i$.
These values satisfies: $\mathbb{T}_{ik}, \mathbb{I}_{ik}, \mathbb{F}_{ik} \in [0, 1]$
Same for C_j:
$\mathbb{T}_{jk}$: True membership degree of $kforC_j$.
$\mathbb{I}_{jk}$: Indeterminacy membership degree of $kforC_j$.
$\mathbb{F}_{jk}$: False membership degree of $kforC_j$.
These values satisfies: $\mathbb{T}_{jk}, \mathbb{I}_{jk}, \mathbb{F}_{jk} \in [0, 1]$.
The cotangent similarity measures between $\mathbb{T}_i$ and C_j is:
$Cotangent_{CSVNS}(T_i, C_j) =$

$$\frac{1}{n}\sum_{k=1}^{n}\{\cot[\frac{\pi}{4} + \frac{\pi}{12}(|\mathbb{T}_{ik} - \mathbb{T}_{jk}| + |\mathbb{I}_{ik} - \mathbb{I}_{jk}| + |\mathbb{F}_{ik} - \mathbb{F}_{jk}|)]\}$$

4.2. Complex Neutrosophic Set-Driven Cotangent Similarity Model for Ambiguous Signal Interpretation

In the contemporary context of surveillance and reconnaissance, one of the biggest challenges is the accurate classification of operational targets $T = \{T_1, T_2, T_3\}$ from observations of multiple (multi-source) signals $S = \{S_1, S_2, S_3\}$ and then the assignment to the most appropriate operational class $C = \{C_1, C_2, C_3\}$ [83].
The data obtained from each target including thermal emissions, radar signatures, electronic intelligence data, and other sensing data is inherently fuzzy, vague and of diverse type. This makes it difficult to capture and manage such ambiguous information in a meaningful way by using conventional mathematical models.
A strong challenge is that a mathematical structure needs to be developed that can encompass degrees of truth, indeterminacy and falsity. Also, the connections between targets, signal sources and operational classes are expressed in terms of event-based measures and their respective evaluations in the operational classification matrix (Table 2), which constitutes a very complex decision-making environment. The parallel response to the raw signal in each target class is generally intractable because there are overlapping feature values, different reliabilities of the measured features, and nonlinearities in the relationships between features. In order to tackle these drawbacks, a CSVNS (Cotangent CSVNS) framework is used to implement a Cotangent Similarity Measure. This is a very effective way to quantify the similarity between every target class pair (T_i, C_j). The proposed measure encompasses the collective effect of the Truth Membership, Indeterminacy Membership and False Membership degrees and normalizes the evaluation over (n = 3) the attributes. This helps to produce detailed similarity scores, which can then be used to compare, rank and match candidate target profiles against the predefined operational class templates. This can help in more robust and informed target classification in the presence of uncertainty and incomplete information.

Table 1: Matrix of Target Intelligence Features Based on Cotangent Similarity $(T \times S)$ [83]

	S_1	S_2	...	S_n
T_1	$\mathbb{T}_{11}, \mathbb{I}_{11}, \mathbb{F}_{11}$	$\mathbb{T}_{12}, \mathbb{I}_{12}, \mathbb{F}_{12}$	...	$\mathbb{T}_{1n}, \mathbb{I}_{1n}, \mathbb{F}_{1n}$
T_2	$\mathbb{T}_{21}, \mathbb{I}_{21}, \mathbb{F}_{21}$	$\mathbb{T}_{22}, \mathbb{I}_{22}, \mathbb{F}_{22}$	...	$\mathbb{T}_{2n}, \mathbb{I}_{2n}, \mathbb{F}_{2n}$
...	...	...	...	...
T_m	$\mathbb{T}_{m1}, \mathbb{I}_{m1}, \mathbb{F}_{m1}$	$\mathbb{T}_{m2}, \mathbb{I}_{m2}, \mathbb{F}_{m2}$	...	$\mathbb{T}_{mn}, \mathbb{I}_{mn}, \mathbb{F}_{mn}$

Table 2: Operational Classification Matrix for Target Surveillance Data $(T \times S \rightarrow C)$ [83]

Row-I	S_1	S_2	S_3	**Row-II**	C_1	C_2	C_3
T_1	$\begin{pmatrix} 0.5e^{\iota\pi(0.6)} \\ 0.7e^{\iota\pi(0.5)} \\ 0.3e^{\iota\pi(0.3)} \end{pmatrix}$	$\begin{pmatrix} 0.6e^{\iota\pi(0.7)} \\ 0.4e^{\iota\pi(0.4)} \\ 0.3e^{\iota\pi(0.4)} \end{pmatrix}$	$\begin{pmatrix} 0.3e^{\iota\pi(0.2)} \\ 0.5e^{\iota\pi(0.5)} \\ 0.8e^{\iota\pi(0.3)} \end{pmatrix}$	S_1	$\begin{pmatrix} 0.3e^{\iota\pi(0.4)} \\ 0.5e^{\iota\pi(0.7)} \\ 0.7e^{\iota\pi(0.7)} \end{pmatrix}$	$\begin{pmatrix} 0.7e^{\iota\pi(0.6)} \\ 0.6e^{\iota\pi(0.5)} \\ 0.2e^{\iota\pi(0.3)} \end{pmatrix}$	$\begin{pmatrix} 0.5e^{\iota\pi(0.8)} \\ 0.4e^{\iota\pi(0.7)} \\ 0.9e^{\iota\pi(0.3)} \end{pmatrix}$
T_2	$\begin{pmatrix} 0.4e^{\iota\pi(0.6)} \\ 0.7e^{\iota\pi(0.9)} \\ 0.5e^{\iota\pi(0.7)} \end{pmatrix}$	$\begin{pmatrix} 0.2e^{\iota\pi(0.4)} \\ 0.4e^{\iota\pi(0.9)} \\ 0.6e^{\iota\pi(0.3)} \end{pmatrix}$	$\begin{pmatrix} 0.7e^{\iota\pi(0.7)} \\ 0.4e^{\iota\pi(0.3)} \\ 0.6e^{\iota\pi(0.6)} \end{pmatrix}$	S_2	$\begin{pmatrix} 0.2e^{\iota\pi(0.5)} \\ 0.3e^{\iota\pi(0.2)} \\ 0.7e^{\iota\pi(0.3)} \end{pmatrix}$	$\begin{pmatrix} 0.6e^{\iota\pi(0.6)} \\ 0.7e^{\iota\pi(0.8)} \\ 0.4e^{\iota\pi(0.3)} \end{pmatrix}$	$\begin{pmatrix} 0.3e^{\iota\pi(0.6)} \\ 0.6e^{\iota\pi(0.7)} \\ 0.8e^{\iota\pi(0.9)} \end{pmatrix}$
T_3	$\begin{pmatrix} 0.7e^{\iota\pi(0.9)} \\ 0.6e^{\iota\pi(0.5)} \\ 0.8e^{\iota\pi(0.8)} \end{pmatrix}$	$\begin{pmatrix} 0.2e^{\iota\pi(0.4)} \\ 0.8e^{\iota\pi(0.5)} \\ 0.7e^{\iota\pi(0.6)} \end{pmatrix}$	$\begin{pmatrix} 0.6e^{\iota\pi(0.9)} \\ 0.3e^{\iota\pi(0.6)} \\ 0.2e^{\iota\pi(0.3)} \end{pmatrix}$	S_3	$\begin{pmatrix} 0.4e^{\iota\pi(0.4)} \\ 0.7e^{\iota\pi(0.5)} \\ 0.5e^{\iota\pi(0.9)} \end{pmatrix}$	$\begin{pmatrix} 0.6e^{\iota\pi(0.2)} \\ 0.3e^{\iota\pi(0.5)} \\ 0.4e^{\iota\pi(0.4)} \end{pmatrix}$	$\begin{pmatrix} 0.7e^{\iota\pi(0.2)} \\ 0.3e^{\iota\pi(0.8)} \\ 0.2e^{\iota\pi(0.3)} \end{pmatrix}$

Calculated values after solving by cotangent formula are:
$Cotangent_{CSVNS}(T_1, C_1) = 0.4913$
$Cotangent_{CSVNS}(T_1, C_2) = 0.6653$

$Cotangent_{CSVNS}(T_1, C_3) = 0.5785$
$Cotangent_{CSVNS}(T_2, C_1) = 0.5287$
$Cotangent_{CSVNS}(T_2, C_2) = 0.4937$
$Cotangent_{CSVNS}(T_2, C_3) = 0.3576$
$Cotangent_{CSVNS}(T_3, C_1) = 0.4110$
$Cotangent_{CSVNS}(T_3, C_2) = 0.4604$
$Cotangent_{CSVNS}(T_3, C_3) = 0.4221$

Table 3: Cotangent Similarity scores between signal samples ($S_1 - S_3$) and class templates ($T_1 - T_3$) [83]

Cot SM	S_1	S_2	S_3
T_1	0.4913	0.6653	0.5785
T_2	0.5287	0.4937	0.3576
T_3	0.4110	0.4604	0.4221

5. Privacy-Preserving Target-Signal Relationship Analysis

In this paper, a privacy-preserving framework for evaluating target-signal interactions using encrypted similarity and correlation metrics is proposed. Sigmoid-based transformations are used to conceal the original values without altering the relative relationships, normalization (0-1 scaling), and comparability of the signals and targets. While privacy-preserving encryption protects sensitive data during computation, the Pearson correlation test quantifies linear relationships. Visualization tools, such as heatmaps (Figures 1-3), bar charts (Figures 4-5), and three-dimensional surface plots (Figures 6-7), which do not display raw numerical values, can be used to communicate encrypted patterns in a way that is easily understandable.

5.1. Sigmoid-Based Encryption Transformation

A nonlinear mathematical procedure is used in the sigmoid transformation encryption alteration to change the original similarity values into masked or protected data. Because it can scale the real-valued input to a narrow range of 0 to 1, the sigmoid curve an S-shaped curve is more often used in statistical modeling and machine learning [84]. It maintains relative rank while distorting the original values' real scale in secure similarity analysis. Because the encrypted function is monotonic, the encrypted outputs increase with the original values. As a result, even while correct numerical data is hidden, the structural relationships within the dataset are preserved. Because relevant patterns shouldn't be concealed in the opaque form of data, the sigmoid-based transformation is particularly appropriate in privacy-preserving systems of analysis [84, 85].

5.2. Normalization (0-1 Scaling)

A preprocessing technique called normalization converts data into a specified range, typically between 0 and 1. This research achieves comparability across various targets and signals by normalizing encrypted similarity and correlation values [86]. Values from different computational levels or measurement scales may generate bias or misinterpretation during comparison or visualization if they are not normalized. It is considerably simpler to analyze when all values fall into a set range: values around 1 have strong correlations, whereas values near 0 have weaker correlations. In order to improve visual clarity and data analytic consistency, normalization would preserve underlying ordering and relative differences between pairs of variables [86].

5.3. Pearson Correlation Analysis

The strength and direction of linear correlations between two variables can be measured using Pearson correlation analysis; the coefficients of Pearson correlation range from -1 to +1. According to [87], positive linear correlation coefficients with a value of +1 are considered positive, negative correlation coefficients with a value of -1 are considered negative, and coefficients with a value of 0 are considered zero. The links between targets (T_1, T_2, T_3) and signals or sources (S_1, S_2, S_3) are examined in this study using Pearson correlation. In order to let researchers identify the predominant relationships and patterns without disclosing the underlying numerical data, sensitive values are encrypted while maintaining the relative correlation structure [85, 87].

5.4. Privacy-Preserving Data Encryption

Data encryption that protects privacy can perform useful calculations and prevent unwanted access to sensitive datasets. This configuration analyzes encrypted numerical numbers, making it impossible for unauthorized parties to replicate the data [85]. Even after encryption, the overall structure of the link between variables remains maintained. This makes it possible for academics to safely perform correlation analysis, similarity analysis, and visualization. These techniques are now essential in a number of economic sectors, including biometric analysis, healthcare, and finance, where data confidentiality is crucial [85].

5.5. Visualization Techniques

When analyzing complex analytical data, the results must be visualized in a way that the viewer can understand. In this instance, a number of methods are employed to construct patterns, trends, and dominant relationships while representing encrypted similarity and correlation values without revealing the original data [88].

5.5.1. Heatmaps

Heatmaps are a visual depiction of matrix data where the values are shown as colors. Higher values are indicated by brighter or warmer ones, whereas lower values are indicated by darker or colder ones [88]. In this study, heatmaps are used to visualize encrypted Cotangent Similarity Measure (CotSM) values and encrypted Pearson correlations between targets and signals. As seen in Figure 1-3 [88], these visual gradients help identify the overwhelming linkages and outliers within the matrix's structure.

5.5.2. Bar Charts

Discrete values, or the strength of encrypted similarity measures between targets and signals, are compared between categories using bar charts. The strongest and weakest correlations are readily discernible, and relative bar heights maintain comparable relationships even when the values are normalized or encrypted. Figures 4 and 5 [89] present these comparisons.

5.5.3. 3D Surface Plots

Three-dimensional surface plots are used to simultaneously show the relationship between multiple variables. Independent variables are defined by two axes, and a third axis such as similarity or correlation is calculated. Strong links are represented by peaks, weaker associations by valleys, and greater interpretability is provided by color gradients [90]. In order to preserve data secrecy while allowing researchers to view multidimensional structures of interaction, this study uses 3D surface plots to show encrypted Pearson correlation values between targets and signals.

Figures 6-7 [90] show these correlations.

6. Result and Discussion

Three targets (T_1, T_2, T_3) and three sources (S_1, S_2, S_3) are compared using heatmaps in Figure 1. Every value indicates how similar a target is to a source, with higher values denoting greater similarity. The cell is circled because the greatest value of 0.4324 lies near the junction of T_1 and S_2. This suggests that T_1 and S_2 have the strongest relationship. Overall, T_1's similarity rating is the highest, indicating that it is the most closely connected of all the sources. T_2 shows a significant degree of resemblance, whereas T_3 shows the least. S_2 is the most potent or dominating source, as evidenced by its higher value across all targets. The relative pattern is preserved even when the data is encrypted. The relationships between the strongest and weakest values are not concealed by encryption, but the individual values are. As a result, T_3 shows the weakest correlations, whereas T_1 and S_2 are the closest. Sensitive data can be safely analyzed using such an encrypted similarity matrix, and the similarity kind of analysis enables comparisons and patterns to be made without disclosing the original numerical data.

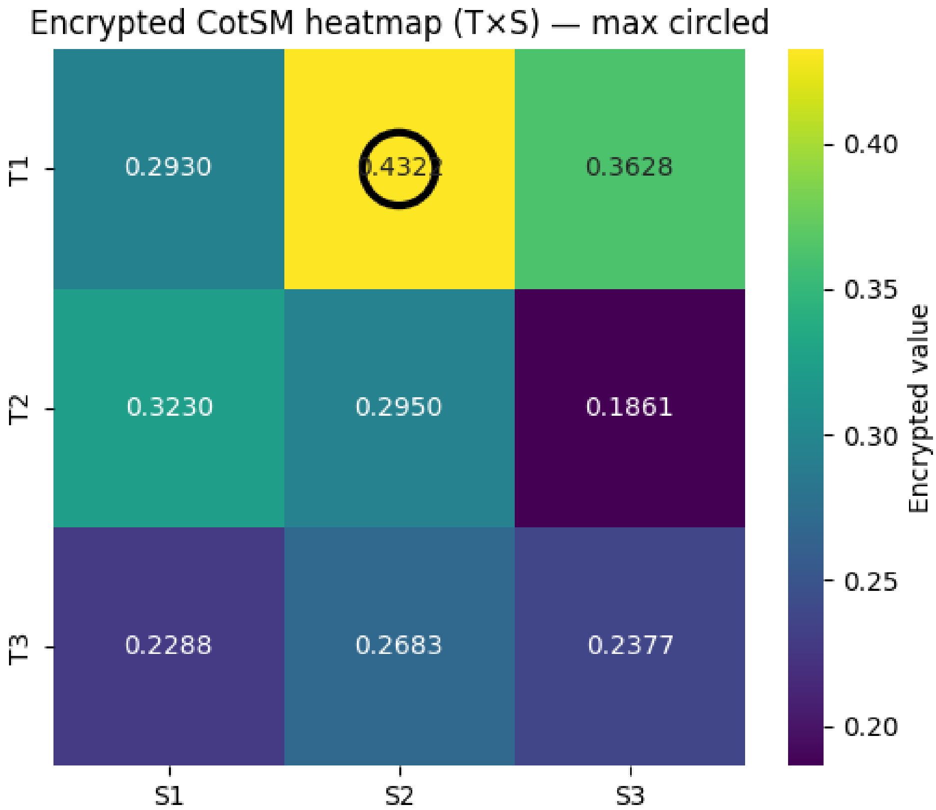

Figure 1: Encrypted Cotangent Similarity (CotSM) Heatmap

Heatmaps are used in Figure 2 above to compare three sources (S_1, S_2, S_3) and three targets (T_1, T_2, T_3). The cells represent the normalized encrypted similarity between a source and a target; higher numbers indicate greater similarity. The cell that is circled has the greatest value, 1.0000, near the junction of T_1 and S_2. This indicates that S_2 and T_1 have the strongest correlation. T_1 is often the most strongly associated with a target and has the highest similarity values with all the sources. T_2 and T_3 have moderate and mild levels of similarity, respectively. S_2 is the most potent or dominant source since it typically records greater values across all targets. The relationship's overall pattern remains unchanged despite the encryption and normalization of the values (01). The underlying similarity structure is preserved while the original numerical data is covered by encryption. T_3 has the weakest correlations, so we can still identify T_1 and S_2 as the closest ones. Because it is possible to see patterns and relationships that do not reveal the raw or sensitive data, the encrypted Cotangent Similarity matrix is particularly useful in a secure comparison analysis.

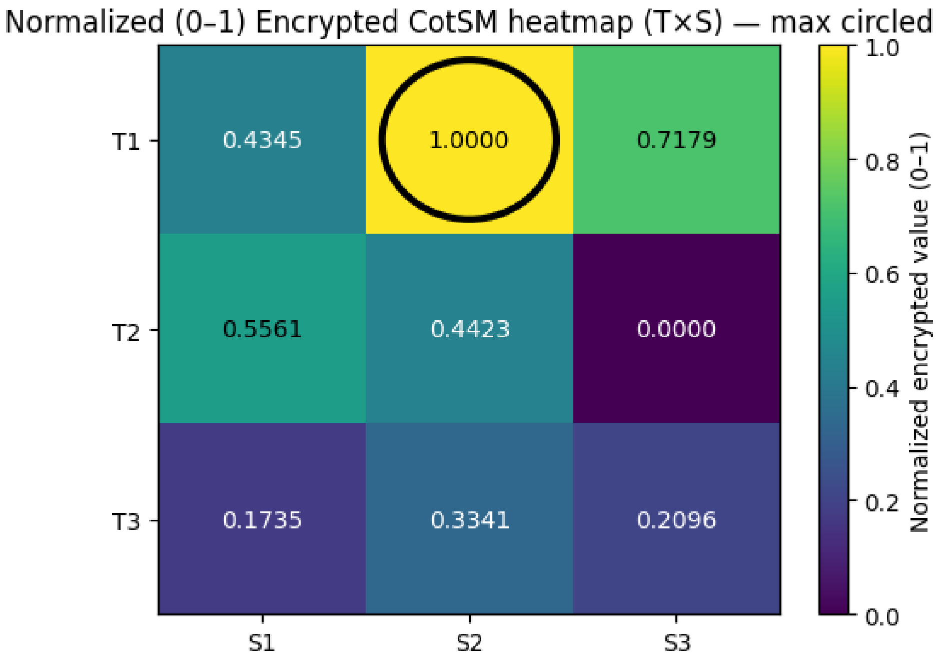

Figure 2: Normalized Encrypted Cotangent Similarity (CotSM) Heatmap

Three sources (S_1, S_2, S_3) and three targets (T_1, T_2, T_3) are compared in Figure 3 (Heatmaps). Each value represents the encrypted Pearson correlation between a source and a target; bigger values suggest a stronger correlation. The cell is ringed because the greatest value of 1.0000 is located at the intersection of T_3 and S_3. This indicates that there is the strongest link between T_3 and S_3. T_3 is the most consistent target overall since it has the highest levels of correlations between the sources. T_2 denotes the weakest relationships, whereas T_1 denotes moderate relationships. In this encrypted correlation space, S_3 appears to be the most potent or dominant source since its values have the highest number of correlations with the targets. The overall pattern of correlation is preserved even with the encrypted data. The structural relationship between variables is preserved even when the operative number values are concealed by encryption. As a result, we can once again clearly see that T_2 has the fewest associations while T_3 and S_3 develop the most.

Because it gives the researcher the chance to examine the linear association and trends of the data without disclosing the original data to jeopardize their privacy, the Encrypted Pearson Correlation matrix is particularly helpful when conducting statistical analysis without disclosing the underlying sensitive data.

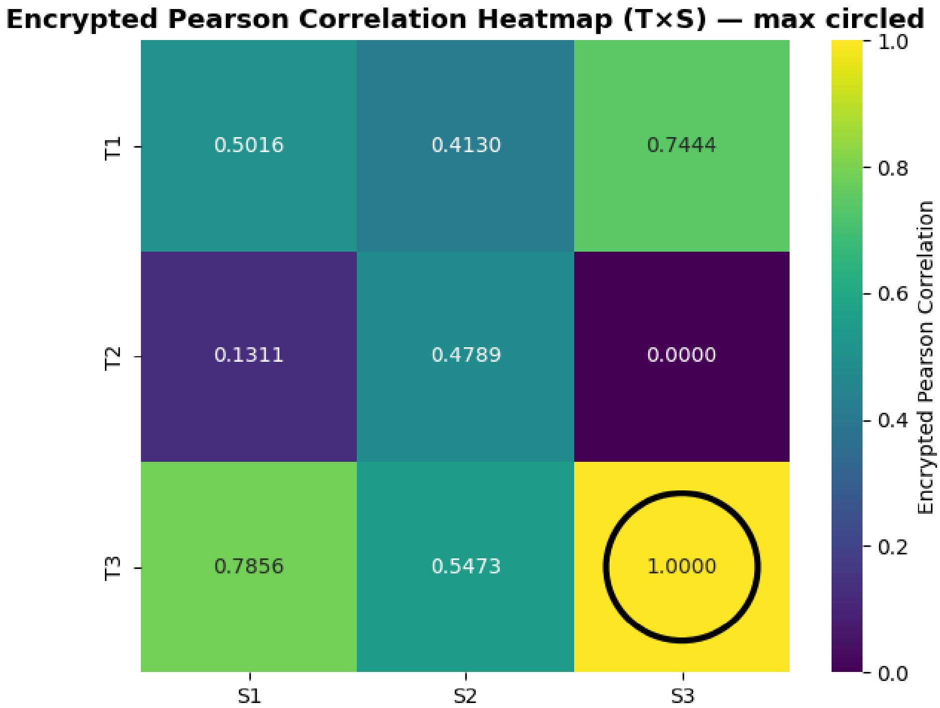

Figure 3: Encrypted Pearson Correlation Heatmap

The bar graph in Figure 4 uses the encrypted Cotangent Similarity Measure (CotSM) under the sigmoid approach to compare three targets (T_1, T_2, T_3) of three signals (S_1, S_2, S_3). Each bar represents the encrypted similarity value between a target and a signal; the larger the bar, the stronger the association. The bar is ringed and marked as MAX since T_1 at S_2 has the highest value of 0.6653. This suggests that S_2 has the strongest association with T_1. Overall, T_1 has consistently displayed the highest encrypted values in the signals, indicating that it is the most dominant target. T_3 has comparatively lower values, while T_2 has a moderate degree of resemblance. S_2 is the strongest signal or the most responsive signal to this encrypted framework since it has the highest collective values of all targets. The sequence of comparisons allows for a complete interpretation of the encrypted numerical data. Encryption preserves the hierarchy of relationships between targets and signals while concealing the true magnitudes. In this manner, we can still identify T_1 S_2 as the strongest combination, whereas T_3 is ultimately the weakest. This Encrypted Cotangent Similarity Bar Graph's goal is to demonstrate how sensitive relational data can be presented in an encrypted way that enables pattern identification and comparative analysis without the need to distribute the actual, unencrypted values.

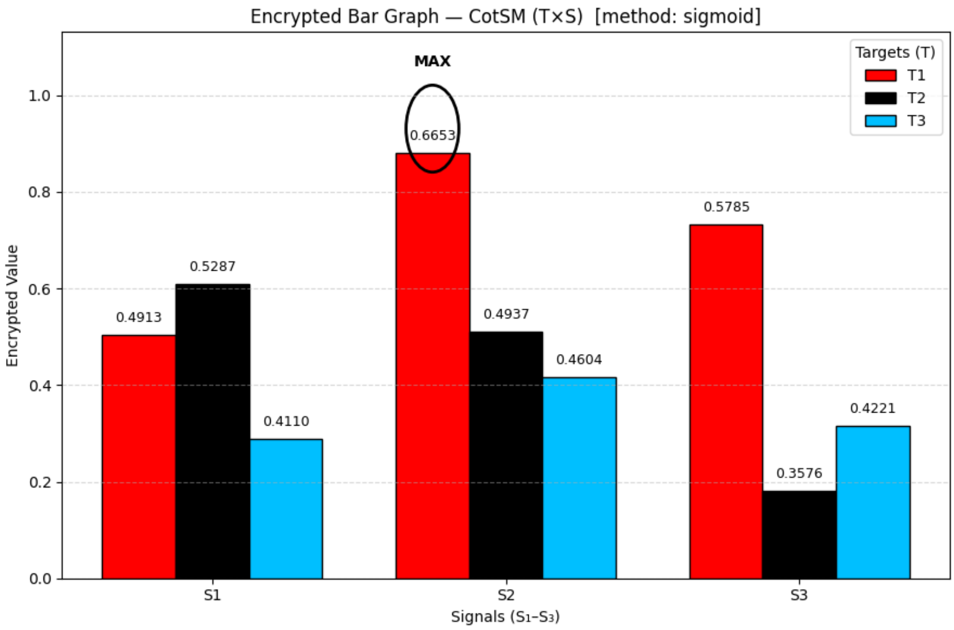

Figure 4: Encrypted Cotangent Similarity (CotSM) Bar Graph using Sigmoid Encryption Method

Three templates (T_1, T_2, T_3) and three signal samples (S_1, S_2, S_3) are discussed in Figure 5 in terms of normalized encrypted Cotangent Similarity Measure (CotSM) values spanning the range of 0 to 1. The bars display the normalized similarity between a signal and an encrypted template; the greater the value, the more similar the two. The most significant correlation in this visualization is found in T_1 in S_2, which has the biggest value, 1.000. Overall, T_1 is the most dominant and highly associated template, as seen by the greatest encrypted signal values of all signals. T_3 consistently has the lowest similarities, while T_2 has medium correlations. S_2 is the most important signal in the encrypted comparison since it has the largest total values across all templates. The relational pattern is retained despite the encryption and normalization of the numerical data. While hiding the true magnitudes, the encryption preserves the relative rank of templates and signals. Because of this, we can easily identify T_1 and S_2 as the most prevalent pair, while T_3 has weaker connections with the other pairs.

In order to examine regularities and comparative strength of the data in the form of a bar chart, this Encoded Cotangent Similarity Bar Chart at normal is particularly helpful when the visualization of sensitive data is required to be safe and maintain the original numerical values undisclosed.

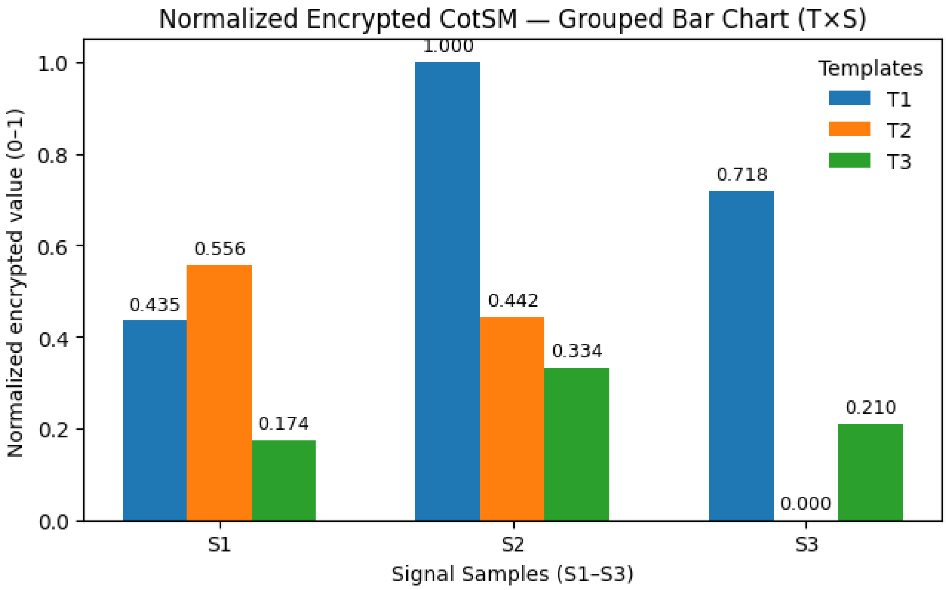

Figure 5: Normalized Encrypted Cotangent Similarity (CotSM) Bar Chart

The encrypted Pearson correlation connections between three targets (T_1, T_2, T_3) and three signals (S_1, S_2, S_3) are plotted on a three-dimensional surface in Figure 6. In order to depict the points on the surface, the brightness of the point represents the strength of the correlation, and the height of the point represents the encrypted Pearson correlation. The strongest connection in the matrix is seen at the intersection of T_3 and S_3, where the highest value of 1.000 is shown by a red dot. Overall, T_3 has the most prominent correlation peaks across the surface, demonstrating its strong association with the signals. The lower and darker portions of the surface indicate that T_2 has the weakest correlations, whereas T_1 is moderate. S_3 consistently had the strongest encrypted correlated responses, and it is reasonable to believe that it had the most impact of all the targets. Despite using a three-dimensional structure the relative relative distance of each target and signal pair the encrypted data maintains the relative correlation topology. While the exact magnitudes are conveyed through encryption, the relationship dynamics there in are maintained. As a result, it is still clear that T_2 is the least associated while T_3 and S_3 are the most closely associated.

When attempting to comprehend the relationships between variables, this Encrypted Pearson Correlation Surface is particularly helpful since it allows us to visualize the correlation structure of variables in a secure environment without revealing any discernible numerical values.

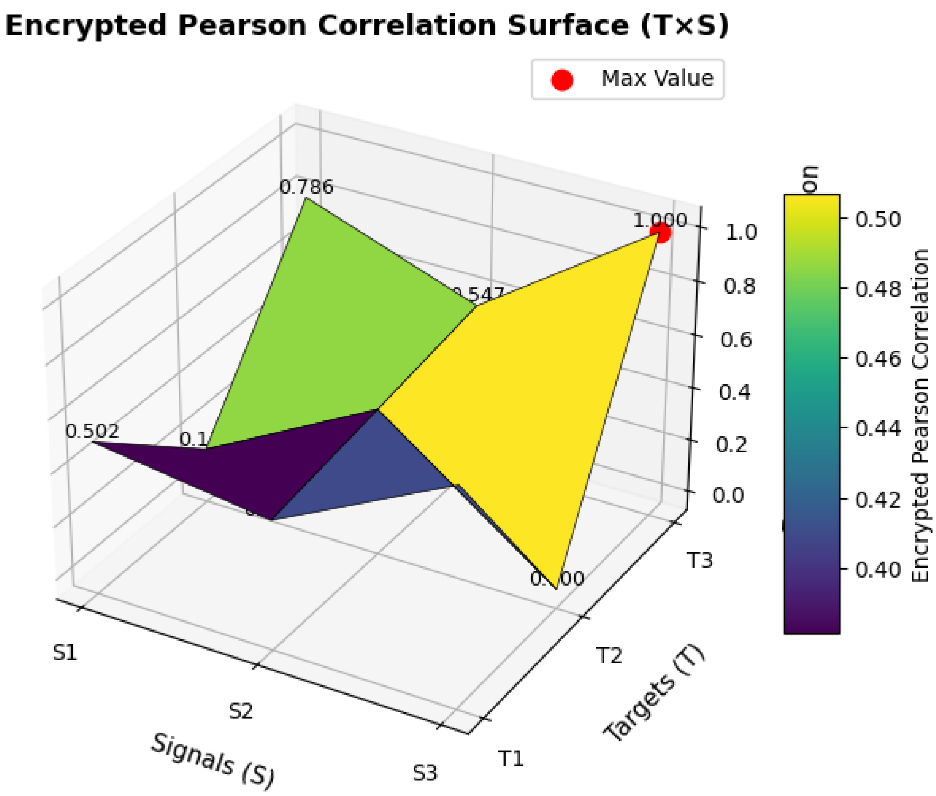

Figure 6: Three-Dimensional Surface Plot of Encrypted Pearson Correlation

The Normalized Encrypted Pearson Correlation of three targets (T_1, T_2, $and\, T_3$) and three signals (S_1, S_2, $and\, S_3$) is plotted in three dimensions in Figure 7. Each surface point represents a normalized encrypted correlation value between 0 and 1; a stronger normalized correlation is shown by a higher peak and brighter color. The intersection of T_1 and S_3 has the greatest value of 1.000, which is shown by a red marker labeled Max (normalized). This indicates that T_1 has the strongest correlation with S_3. Overall, T_1 exhibits the strongest normalized encrypted response and the most dominant correlation intensity. T_2 and T_3 are less connected to every signal and have a more flattened surface. S_3 has the highest normalized correlation value among the targets since it is the most sensitive signal. The required correlation pattern is preserved even after the dataset has been normalized and encrypted. Normalization is used to make the data appear comparable while encryption blurs the true magnitudes. The $T_1 S_3$ pair is the best normalized pair, and the relationship integrity is maintained. The associations of the other pairs are nearly zero. It is a tested visualization that is very helpful for precisely interpreting patterns without revealing the original numerical values when seeing the distribution and strengths of encrypted correlations in a secure analytical environment.

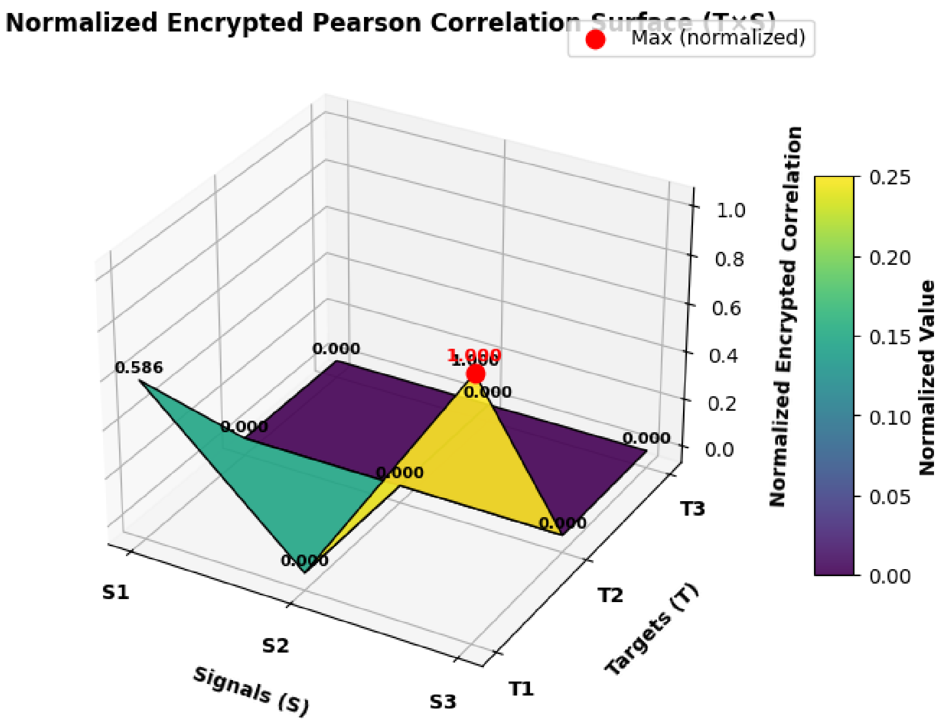

Figure 7: Three-Dimensional Surface Plot of Normalized Encrypted Pearson Correlation

7. Comparative Visualization of Raw and Normalized Encrypted Cotangent Similarity Measures across Targets and Signals

In this study, three-target and three-signal bar graphs in 2D and 3D formats are used to easily compare and display the raw and normalized values of the encrypted Cotangent Similarity Measure (CotSM). Without sacrificing the relative ordering, normalization reduces the scales to a range of 0 to 1, making understanding easier. The strongest correlation is consistently found between dominating couples, particularly T_1 S_2 and T_2 S_1. The color schemes and numerical annotations effectively highlight these patterns, demonstrating the method's suitability for safe pattern identification and privacy-preserving analysis.

The bar graph in Figure 8 below provides a clear comparison of the raw and normalized encrypted Cotangent Similarity Measure (CotSM) values of three signals (S_1, S_2, S_3) and three targets (T_1, T_2, T_3). The highest MAX mark above the bar strongly highlights the maximum normalized value of 1.000 at T_1-S_2. T_1 -S_2 has the biggest raw value of 0.432, confirming the supremacy of this pair even before normalizing. The other notable maximum normalized value is 0.745 at T_2 -S_1, which is likewise designated as MAX. Because the higher visual comparison is simpler, scaling in the 01 range raises normalized values relative to raw data. The relative ranks remain same with this scale, with T_1 having the best relationships among signals, followed by T_2, and T_3. Normalization improves interpretability without changing the underlying structural relationships since it maintains the pattern.When examining the targets, T_1 is consistently the most associated, especially with S_2. The values of T_2 are moderate and have a strong high point at S_1, while the values of T_3 are the lowest in both raw and normalized values. The strongest signal is S_2, which has the highest normalized values for all targets, particularly the T_1 scenario. Signals S_1 and S_3 have moderate to low similarity scores, with S_3 usually being the weakest target. The graph is simpler to visualize when certain hatching colors and patterns are used to easily distinguish between the raw and normalized numbers. The readability is improved by the numbers at the top of each bar, and the annotations of the most notable pairs are useful for quickly displaying the most significant observations. Overall, this graph indicates that normalizing encrypted similarity metrics might improve their interpretability without compromising the data's comparative integrity. The method's suitability for privacy-sensitive analysis and safe pattern recognition between targets and signals is confirmed by a robust and consistent correlation between T_1 and S_2.

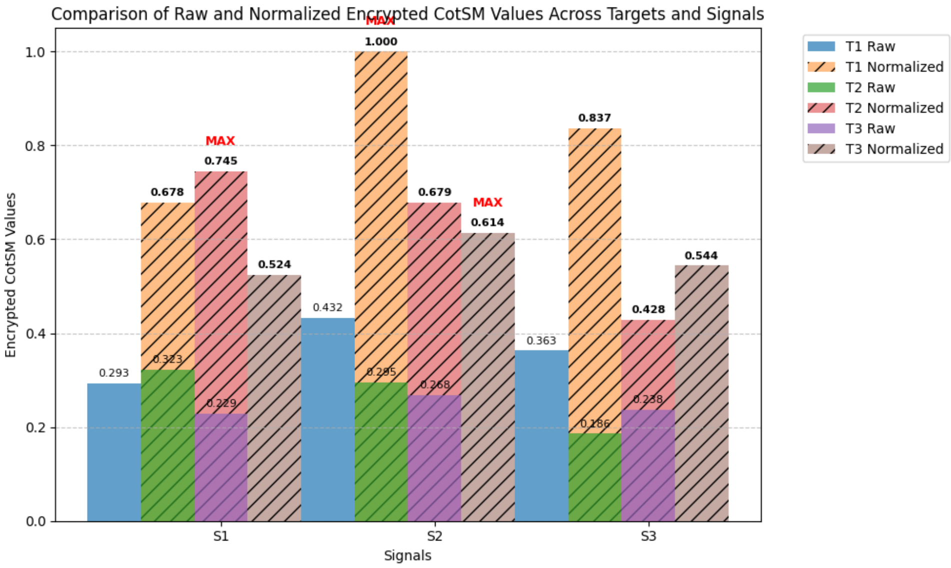

Figure 8: Encrypted Cotangent Similarity Comparison Before and After Normalization

A close-up comparison of the raw and normalized values of the encrypted Cotangent Similarity Measure (CotSM) between three targets (T_1, T_2, T_3) and three signals (S_1, S_2, S_3) is shown in Figure 9, a 3D bar graph. Using several color schemes, the graph effectively differentiates between raw and normalized data: the light and translucent colors (pink for T_1, yellow for T_2, and lavender for T_3) and the solid and deeper colors (red for T_1, orange for T_2, and purple for T_3) indicate raw. Viewers can compare the two sets of data simultaneously in the same 3D area thanks to this visual separation. As can be seen on the top of the pink bar, T_1-S_2 has the greatest normalized value of 1.000 among all the pairs between the targets and signals, making it the most dominating normalized similarity. Additionally, there is a relatively high normalized value of T_3 (0.524-0.614) and a large normalized T_2S_1 of 0.745. The raw value of T_1 S_2 is roughly 0.432, which is consistent with the results of normal and raw scores. Although raw values are often lower since they reflect the original scale, they share the same relative trend. The target analyzing trend shows a consistent pattern with T_1 dominance, and T_1 compares best with signal S_2. T_2 and S_1 have somewhat similar levels of similarity, with S_1 having the highest similarity and T_3 having the lowest. Out of all the targets, S_2 is the most effective signal, followed by S_1 and S_3. An overview of the fluctuation in similarity values between targets, signals, and data types (raw or normalized) at the same time can be easily obtained with the 3D format. It is able to accurately compare each value at a glance thanks to the numerical labels on each bar, which enhance the level of clarity.

Overall, this graphic demonstrates that normalization improves interpretability rather than altering the relative placements of encrypted CotSM values. The power of this privacy-preserving similarity analysis between the targets and signals is confirmed by the clear display of dominating pairs, such as T_1S_2 and T_2S_1.

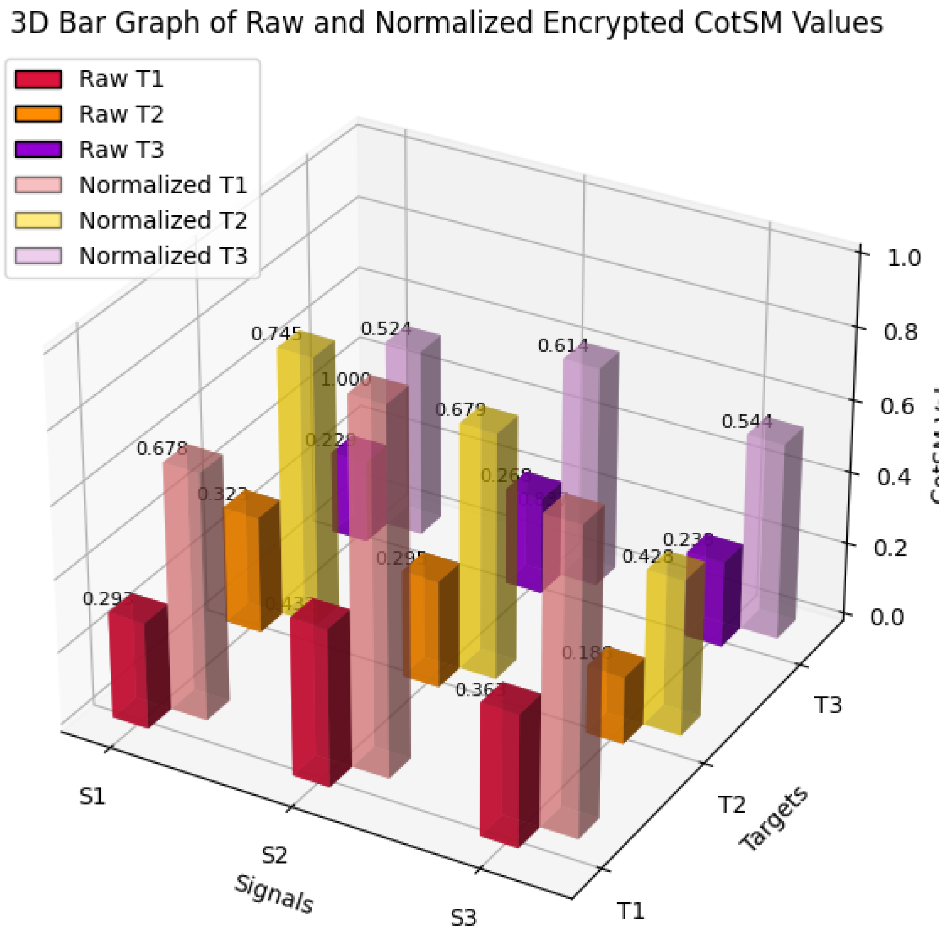

Figure 9: Three-Dimensional Bar Graph of Raw and Normalized Encrypted Cotangent Similarity (CotSM) Values

8. Aspect-Method Hybrid Analysis of Encrypted Cot similarity Measure

Aspect-based reading (pairwise maxima, target dominance, source influence, and invariance under normalization) and method-based evaluation (CotSM vs. Pearson contrast, rank-preserving encoding, 01 normalization, and cross-view checks using heatmaps, bar charts, and 3D surfaces) provide a thorough understanding of signal-template alignment. Because a target may appear powerful in one lens (CotSM: T_1-S_2) and weak in another (Pearson: T_3-S_3), conclusions are never drawn from a single measure or plot in this mixed design. Order-preserving encoding allows for auditable comparison and rapid validation utilizing rank tests and argmax agreement by concealing magnitudes and maintaining rankings. The complementing nature and methodology improve results, promptly show errors (such as incorrectly labeled normalized views), and offer proof of privacy and decision-making abilities without disclosing raw values.

8.1. Aspect-based Analysis

The most important one in CotSM (Figs. 1, 2, 4, 5) is T_1S_2 (0.4324 in the heatmap; 0.6653 in bars; 1.000 when normalized). According to Pearson, the pair T_3S_3 (Figs. 3, 6) has the best value (1.000), which is regarded as the highest cell and a tallest ridge. Pearson has T_3 dominance, T_1 mid-weak, and T_2 mid-weak, while CotSM has T_1 dominance, T_2 dominance, and T_3 dominance. Sources state that Pearson refers to S_3, but CotSM asserts that S_2 is the most significant. The order remains unchanged after normalizing to [0,1]: CotSM is still T_1S_2

with T_1S_2 being the largest, and Pearson should be T_3S_3 with T_3S_3 being the largest. The comparative story (who wins, who follows) is nevertheless fully accessible because encryption hides magnitudes while maintaining ranks. Note: The text in Figure 7 says that the normalized Pearson's maximum is at T_1S_3, which is inconsistent with Figures 3 and 6. This suggests a normalization, labeling, or caption issue, which should be fixed, but the normalized matrix should also be provided.

8.2. Method-based Analysis

CotSM and Pearson prefer T_1-S_2 and T_3-S_3, respectively, without claiming that either is true since CotSM and Pearson fill separate boxes: the former captures similarity in the geometric representations, while the latter captures similarity in the linear representations. Heatmaps, bars, and surfaces all concur that there are victors and losers even with obfuscated numbers since the strictly monotone rank-preserving map keeps the argmax/min and the complete ordering unaltered. Your CotSM numbers and the Pearson set should not be reversed by the visual rescale, minmax to [0,1]. This is because Figure 7 claims that T_1S_3 is the most likely value, which suggests a labeling or processing problem. Cross-referencing Heatmaps with bars (CotSM): Heatmaps with bars show the same row/column dominance and maxima. Heatmaps and 3D surfaces (Pearson): Heatmaps that correspond to column dominance maxima and peak locations are easily recognized. Quick validation Verify that argmax agrees with all CotSM views (T_1-S_2) and all Pearson views (T_3-S_3) by calculating the Spearman/Kendall of raw, normalized, and encrypted matrices (should be 1.0). Examine the modes of failure. False 3D interpolation, per-figure normalization with mismatched anchors, and coarse rounding to quantization ties, per-figure normalization can tie the values of several anchors and make the values of various anchors deceptive, while coarse rounding can tie the quantization levels of a specific number. Per-figure normalization can bind the levels of the various anchors and make the levels of the various anchors deceptive, whereas coarse rounding can tie the quantization levels of a particular number. The quantization levels of coarse rounding can be tied to the bottom line, the narrative is cohesive.

8.3. Normalized Analysis

Since encrypted values are transformed into the standard range, the normalization technique (0-1 scaling) facilitates the comparison of targets and signals. While maintaining the relative position of the values in the transformation, it is simpler to visually identify dominant relationships. For example, T_1S_2's superior relationship is supported by the biggest normalized CotSM of 1.000; however, T_2 consistently shows relatively weak correlations in normalized measures, which are comparable to the patterns in the original encrypted data. Normalization improves visual representation and simplifies the interpretation of encrypted data, even if it does not alter the fundamental ranks.

8.4. Sensitivity Analysis

Sensitivity analysis assesses how sensitive encrypted similarity and correlation patterns are in situations where data or parameter settings are not significantly altered. The investigation shows that signal pairings and dominating target pairs, such as T_1S_2 and T_3S_3, remain unchanged after many encryptions. There is little change in the normalized and raw encrypted measures, which suggests that the computed values are quite stable. Furthermore, even slight changes in data scale or encryption parameters, the structural associations that is, the ranking of the strongest to the weakest relationships remain intact. The results confirm that the privacy-preserving model is resilient to minor perturbations to produce reliable and understandable outcomes; hence, the analytical conclusions drawn from encrypted data may be relied upon.

9. Conclusion

In the Complex Neutrosophic Set (CNS) scenario, we have provided one privacy-conscious visual analytics method of the paired targetsource relations. The estimates of Cotangent Similarity (CotSM) and Pearson correlation are applied to CNS representations that are encoded using strictly monotone and rank-preserving encoding. These representations include encrypted Heatmaps, a grouped bar chart, and raw, minmax normalized 3D surfaces. Empirically, CotSM consistently increases T_1 (e.g., Heatmaps 0.4324, bar 0.6653, normalized 1.000), while Pearson increases T_3 (normalized 1.000). The lessons are obvious: (1) Hidden magnitudes do not damage the encoding, which preserves relative ranks, ordering maximum, minimum, and comparative interpretation. (2) The choice of measurements affects the story. CotSM is comparable to geometric (T_1-S_2), whereas Pearson is comparable to linear (T_3-S_3). Normalization and 3D re-expression only refer to rescaling and reframing, not hierarchy modification. In practical terms, this offers a safe and interpretable framework for signal-template matching, model selection, and sensitive CNS-data pattern finding. Limit: order leakage cannot be prevented; otherwise, stronger OPE/ORE or enclave-based computation is needed if rank secrecy is desired.

10. Future Work

The job is simple: assess differential privacy of ranks where the amount of noise required to ensure top-k is high probability; apply OPE/ORE grade structures or perform CotSM/Pearson inside TEEs (SGX/SEV) and publish merely order/argmax to make privacy tougher. Use adaptive precision k or order-only tokens (no spacing) to make encoding tie-robust, and show probabilistic limitations on the rank-flip probability future. Incorporate uncertainty layers that are calculated directly from encrypted results, such as rank-stability curves, bootstrap CIs, and rank gap permutation tests. Govern metrics can be multi-objective (such as a CotSM-Pearson Pareto front) or have a clearly stated selection process with regard to task utility, stability, and domain bias. They can also compare alternatives (such as Spearman, distance correlation, HSIC, and complex-cosine). Incorporate identifiability tests, publish ablations (remove phase/exchange t-norm with measure impact), and carefully calibrate CNS using T, I, and F construction (phase policies, t-norms, and t-conorms). T and S computation on a large scale With incremental updates, streaming rank maintenance using encrypted top k query APIs, and sparse/block processing, scale to enormous $T \times S$. Use global, rank-only heatmaps (no numbers), uncertainty overlays, no smoothing in 3D, row/column based normalizations, and interactive drill downs to make visuals safer. Ensure cross-run comparability To guarantee cross-run comparability and prevent raw scale leaking, adjust reference anchors (quantile pins or shared min/max). Formal assaults include frequency and known/chosen-plaintext attacks, as well as publishing worst-case Finally, contrast public protocols, code, and pre-registered metrics (AUC, top-k accuracy, Kendall-value, rank stability under noise) with real CNS applications (ECG/EEG, radar, seasonal recommenders) on real data (protocols, code, pre-registered metrics, AUC, top-k accuracy, Kendall-value, rank stability in the presence of noise). For future work, neutrosophic soft sets could model the indeterminacy in non-Hermitian topological phase transitions and the robustness of Majorana modes [80].

Authors' Contributions: All the authors contributed significantly in writing this article. The authors read and approved the final manuscript.
Competing Interests: The authors declare that they have no competing interests.

References

[1] N. H. Phuong, V. V. Thang, and K. Hirota. Case based reasoning for medical diagnosis using fuzzy set theory. *International Journal of Biomedical Soft Computing and Human Sciences*, 5(2):1–7, 2000.

[2] G. Shahzadi, M. Akram, and A. B. Saeid. An application of single-valued neutrosophic sets in medical diagnosis. *Neutrosophic Sets and Systems*, 18:80–88, 2017.

[3] O. J. Tobias and R. Seara. Image segmentation by histogram thresholding using fuzzy sets. *IEEE Transactions on Image Processing*, 11(12):1457–1465, 2002.

[4] K. T. Atanassov. Intuitionistic fuzzy sets. *Fuzzy Sets and Systems*, 20:87–96, 1986.

[5] F. Smarandache. *Neutrosophy: Neutrosophic Probability, Set and Logic*. American Research Press, Mexico, 1998.

[6] F. Smarandache. *A Unifying Field in Logics, Neutrosophy: Neutrosophic Probability, Set and Logic*. American Research Press, Mexico, 1999.

[7] H. Wang, F. Smarandache, Y. Q. Zhang, and R. Sunderraman. Single valued neutrosophic sets. *Multispace and Multistructure*, 4:410–413, 2010.

[8] H. Wang, F. Smarandache, Y. Q. Zhang, and R. Sunderraman. *Interval Neutrosophic Sets and Logic: Theory and Applications in Computing*. Hexis, Phoenix, 2005.

[9] J. J. Peng, J. Wang, J. Wang, H. Zhang, and X. Chen. Simplified neutrosophic sets and their applications in multi-criteria group decision-making problems. *International Journal of Systems Science*, 47(10):2342–2358, 2016.

[10] P. K. Maji. Neutrosophic soft set. *Annals of Fuzzy Mathematics and Informatics*, 5(1):157–168, 2013.

[11] M. Ali and F. Smarandache. Complex neutrosophic set. *Neural Computing and Applications*, 28(7):1817–1834, 2017.

[12] J. Ye. An extended topsis method for multiple attribute group decision making based on single valued neutrosophic linguistic numbers. *Journal of Intelligent & Fuzzy Systems*, 28(1):247–255, 2015.

[13] Z. P. Tian, J. Q. Wang, and H. Y. Zhang. Simplified neutrosophic linguistic normalized weighted bonferroni mean operator and its application to multi-criteria decision-making problems. *Filomat*, 30(12):3339–3360, 2016.

[14] J. Q. Wang and X. E. Li. An application of the todim method with multi-valued neutrosophic set. *Control and Decision*, 30(6):1139–1142, 2015.

[15] S. Broumi, F. Smarandache, and M. Dhar. Rough neutrosophic set. *Italian Journal of Pure and Applied Mathematics*, 32:493–502, 2014.

[16] Y. B. Jun, F. Smarandache, and C. S. Kim. Neutrosophic cubic sets. *New Mathematics and Natural Computation*, 13(1):41–54, 2017.

[17] M. Gulistan and S. Khan. Extentions of neutrosophic cubic sets via complex fuzzy sets with application. *Complex & Intelligent Systems*, 6:309–320, 2020.

[18] C. Bonferroni. Sulle medie multiple di potenze. *Bolletino dell'Unione Matematica Italiana*, 5(3–4):267–270, 1950.

[19] R. R. Yager. The power average operator. *IEEE Transactions on Systems, Man, and Cybernetics - Part A: Systems and Humans*, 31(6):724–731, 2001.

[20] R. R. Yager. Prioritized aggregation operators. *International Journal of Approximate Reasoning*, 48(1):263–274, 2008.

[21] J. Dombi. A general class of fuzzy operators, the demorgan class of fuzzy operators and fuzziness measures induced by fuzzy operators. *Fuzzy Sets and Systems*, 8(2):149–163, 1982.

[22] E. K. Zavadskas, R. Bausys, and M. Lazauskas. Sustainable assessment of alternative sites for the construction of a waste incineration plant by applying waspas method with single-valued neutrosophic set. *Sustainability*, 7(12):15923–15936, 2015.

[23] A. Vafadarnikjoo, N. Mishra, K. Govindan, and K. Chalvatzis. Assessment of consumers'

motivations to purchase a remanufactured product by applying fuzzy delphi method and single valued neutrosophic sets. *Journal of Cleaner Production*, 196:230–244, 2018.

[24] S. Broumi, P. K. Singh, M. Talea, A. Bakali, F. Smarandache, and V. V. Rao. Single-valued neutrosophic techniques for analysis of wifi connection. In *Advances in Intelligent Systems and Sustainable Development*, volume 915, pages 405–412. 2018.

[25] G. Selvachandran, S. G. Quek, F. Smarandache, and S. Broumi. An extended technique for order preference by similarity to an ideal solution (topsis) with maximizing deviation method based on integrated weight measure for single-valued neutrosophic sets. *Symmetry*, 10(7):236–252, 2018.

[26] P. Biswas, S. Pramanik, and B. C. Giri. Non-linear programming approach for single-valued neutrosophic topsis method. *New Mathematics and Natural Computation*, 15(2):307–326, 2019.

[27] M. Abdel-Basset, M. Ali, and A. Atef. Uncertainty assessments of linear time-cost tradeoffs using neutrosophic set. *Computers & Industrial Engineering*, 141:106286, 2020.

[28] M. Abdel-Basset and R. Mohamed. A novel plithogenic topsis-critic model for sustainable supply chain risk management. *Journal of Cleaner Production*, 247:119586, 2020.

[29] M. Abdel-Basset, M. Ali, and A. Atef. Resource levelling problem in construction projects under neutrosophic environment. *The Journal of Supercomputing*, 76:964–988, 2020.

[30] M. Akram, S. Naz, and F. Smarandache. Generalization of maximizing deviation and topsis method for madm in simplified neutrosophic hesitant fuzzy environment. *Symmetry*, 11(8):1058, 2019.

[31] J. Zhan, M. Akram, and M. Sitara. Novel decision-making method based on bipolar neutrosophic information. *Soft Computing*, 23(20):9955–9977, 2019.

[32] M. Aslam. Neutrosophic analysis of variance: Application to university students. *Complex & Intelligent Systems*, 5(4):403–407, 2019.

[33] I. R. Sumathi and C. A. C. Sweety. New approach on differential equation via trapezoid neutrosophic number. *Complex & Intelligent Systems*, 5(4):417–424, 2019.

[34] S. Broumi and F. Smarandache. Several similarity measures of neutrosophic sets. *Neutrosophic Sets and Systems*, 1:54–62, 2013.

[35] J. Ye. Multicriteria decision-making method using the correlation coefficient under single-valued neutrosophic environment. *International Journal of General Systems*, 42(4):386–394, 2013.

[36] J. Ye. A multicriteria decision-making method using aggregation operators for simplified neutrosophic sets. *Journal of Intelligent & Fuzzy Systems*, 26(5):2459–2466, 2014.

[37] J. Ye. Vector similarity measures of simplified neutrosophic sets and their application in multicriteria decision making. *International Journal of Fuzzy Systems*, 16(2):204–211, 2014.

[38] J. Ye. Clustering methods using distance-based similarity measures of single-valued neutrosophic sets. *Journal of Intelligent Systems*, 23(4):379–389, 2014.

[39] J. Ye. Improved cosine similarity measures of simplified neutrosophic sets for medical diagnoses. *Artificial Intelligence in Medicine*, 63(3):171–179, 2015.

[40] J. Ye. Single-valued neutrosophic clustering algorithms based on similarity measures. *Journal of Classification*, 34(1):148–162, 2017.

[41] J. Ye and Q. S. Zhang. Single valued neutrosophic similarity measures for multiple attribute decision making. *Neutrosophic Sets and Systems*, 2:48–54, 2014.

[42] J. Ye. Single-valued neutrosophic similarity measures based on cotangent function and their application in the fault diagnosis of steam turbine. *Soft Computing*, 21(3):817–825, 2017.

[43] P. Majumdar and S. K. Samanta. On similarity and entropy of neutrosophic sets. *Journal of Intelligent & Fuzzy Systems*, 26(3):1245–1252, 2014.

[44] K. Mondal and S. Pramanik. Neutrosophic tangent similarity measure and its application

to multiple attribute decision making. *Neutrosophic Sets and Systems*, 9:80–87, 2015.

[45] J. Ye and J. Fu. Multi-period medical diagnosis method using a single valued neutrosophic similarity measure based on tangent function. *Computer Methods and Programs in Biomedicine*, 123:142–149, 2016.

[46] C. F. Liu and Y. S. Luo. The weighted distance measure based method to neutrosophic multiattribute group decision making. *Mathematical Problems in Engineering*, 2016:3145349, 2016.

[47] H. L. Huang. New distance measure of single-valued neutrosophic sets and its application. *International Journal of Intelligent Systems*, 31(10):1021–1032, 2016.

[48] K. Mandal and K. Basu. Improved similarity measure in neutrosophic environment and its application in finding minimum spanning tree. *Journal of Intelligent & Fuzzy Systems*, 31(3):1721–1730, 2016.

[49] H. Garg and Nancy. Some new biparametric distance measures on single-valued neutrosophic sets with applications to pattern recognition and medical diagnosis. *Information*, 8(4):162, 2017.

[50] S. Pramanik, P. Biswas, and B. C. Giri. Hybrid vector similarity measures and their applications to multi-attribute decision making under neutrosophic environment. *Neural Computing and Applications*, 28(5):1163–1176, 2017.

[51] M. Sahin, N. Olgun, V. Ulucay, A. Kargin, and F. Smarandache. A new similarity measure based on falsify value between single valued neutrosophic sets based on the centroid points of transformed single valued neutrosophic numbers with applications to pattern recognition. *Neutrosophic Sets and Systems*, 15:31–48, 2017.

[52] J. Fu and J. Ye. Simplified neutrosophic exponential similarity measures for the initial evaluation/diagnosis of benign prostatic hyperplasia symptoms. *Symmetry*, 9(8):154, 2017.

[53] H. Wu, Y. Yuan, L. Wei, and L. Pei. On entropy, similarity measure and cross-entropy of single-valued neutrosophic sets and their application in multi-attribute decision making. *Soft Computing*, 22(22):7367–7376, 2018.

[54] W. Cui and J. Ye. Improved symmetry measures of simplified neutrosophic sets and their decision making method based on a sine entropy weight model. *Symmetry*, 10(6):225, 2018.

[55] K. Mondal, S. Pramanik, and B. C. Giri. Hybrid binary logarithm similarity measure for magdm problems under svns assessments. *Neutrosophic Sets and Systems*, 20:12–15, 2018.

[56] K. Mondal, S. Pramanik, and B. C. Giri. Single valued neutrosophic hyperbolic sine similarity measure based strategy for madm problems. *Neutrosophic Sets and Systems*, 20:3–11, 2018.

[57] C. Liu. New similarity measures of simplified neutrosophic sets and their applications. *Journal of Information Processing Systems*, 14(3):790–800, 2018.

[58] D. Liu, G. Liu, and Z. Liu. Some similarity measures of neutrosophic sets based on the euclidean distance and their application in medical diagnosis. *Computational and Mathematical Methods in Medicine*, 2018:8618135, 2018.

[59] R. Sun, J. Hu, and X. Chen. Novel single-valued neutrosophic decision-making approaches based on prospect theory and their applications in physician selection. *Soft Computing*, 23(1):211–225, 2019.

[60] X. Peng and F. Smarandache. New multiparametric similarity measure for neutrosophic set with big data industry evaluation. *Artificial Intelligence Review*, 53:3089–3125, 2020.

[61] H. P. Ren, S. X. Xiao, and H. Zhou. A chi-squared distance-based similarity measure of single-valued neutrosophic set and applications. *International Journal of Computers Communications & Control*, 14(1):78–89, 2019.

[62] A. Aydogdu. On similarity and entropy of single valued neutrosophic sets. *General Mathematics Notes*, 29(1):67–74, 2015.

[63] H. Garg and A. Nancy. On single-valued neutrosophic entropy of order α. *Neutrosophic Sets and Systems*, 14:21–28, 2016.

[64] W. Cui and J. Ye. Generalised distance-based entropy and dimension root entropy for simplified neutrosophic sets. *Entropy*, 20(11):844, 2018.

[65] A. Aydogdu and R. Sahin. New entropy measures based on neutrosophic set and their applications to multi-criteria decision making. *Journal of Natural & Applied Sciences*, 23(1):40–45, 2019.

[66] R. Hatamleh, A. Al-Husban, N. Sundarakannan, and M. S. Malchijah Raj. Complex cubic intuitionistic fuzzy set applied to subbisemirings of bisemirings using homomorphism. *Communications on Applied Nonlinear Analysis*, 32(3):418–435, 2025.

[67] R. Hatamleh, A. Al-Husban, Sundareswari, G. K. Balaj, and M. Palanikumar. Complex tangent trigonometric approach applied to (γ, τ)-rung fuzzy set using weighted averaging, geometric operators and its extension. *Communications on Applied Nonlinear Analysis*, 32(5):133–144, 2025.

[68] R. Hatamleh and A. Hazaymeh. Finding minimal units in several two-fold fuzzy finite neutrosophic rings. *Neutrosophic Sets and Systems*, 70:1–16, 2024.

[69] R. Hatamleh and A. Hazaymeh. On some topological spaces based on symbolic n plithogenic intervals. *International Journal of Neutrosophic Science*, 25(1):23–37, 2025.

[70] S. A. El-Sheikh and A. M. Abd El-Latif. Decompositions of some types of supra soft sets and soft continuity. *International Journal of Mathematics Trends and Technology*, 9(1):37–56, 2014.

[71] A. M. Abd El-Latif. Soft supra strongly generalized closed sets. *Journal of Intelligent & Fuzzy Systems*, 31(3):1311–1317, 2016.

[72] A. M. Abd El-Latif and R. A. Hosny. Soft supra extra strongly generalized closed sets. *Analele Universitatii din Oradea Fascicola Matematica*, 24(1):103–112, 2017.

[73] A. M. Abd El-Latif. Soft supra strongly $semi^*$ generalized closed sets. *Annals of Fuzzy Mathematics and Informatics*, 13(1):63–71, 2017.

[74] A. M. Abd El-Latif. Supra soft b-connectedness ii: Some types of supra soft b-connectedness. *Creative Mathematics and Informatics*, 26(1):1–8, 2017.

[75] A. M. Abd El-Latif and R. A. Hosny. Supra open soft sets and associated soft separation axioms. *International Journal of Advanced Mathematics*, 6:68–81, 2017.

[76] A. M. Abd El-Latif and R. A. Hosny. Supra soft separation axioms and supra irresoluteness based on supra b-soft sets. *Gazi University Journal of Science*, 29(4):845–854, 2016.

[77] A. M. Abd El-Latif and R. A. Hosny. Supra semi open soft sets and associated soft separation axioms. *Applied Mathematics and Information Sciences*, 10(6):2207–2215, 2016.

[78] A. M. Abd El-Latif and S. Karatas. Soft supra strongly generalized closed sets via soft ideals. *Applied Mathematics and Information Sciences Letters*, 5(1):21–26, 2016.

[79] A. M. Abd El-Latif. On soft supra compactness in supra soft topological spaces. *Tbilisi Mathematical Journal*, 11(1):169–178, 2018.

[80] X. Ji, H. Geng, N. Akhtar, and X. Yang. Floquet engineering of point-gapped topological superconductors. *Physical Review B*, 111(19):195419, 2025.

[81] X. Yang, Y. Feng, Abdul Wahab, and H. Geng. Non-hermitian second-order topological phases and bipolar skin effect in photonic kagome crystals. *Physical Review A*, 113:023506, 2026.

[82] M. Ali and F. Smarandache. Complex neutrosophic set. *Neural Computing and Applications*, 25:1–18, 2016.

[83] H. Qawaqneh, W. M. M. Salameh, D. A. M. Mahmoud, G. Nordo, A. Hussain, A. Mehmood, and C. L. Armada. Structure-preserving clustering in encrypted feature spaces. *Statistics, Optimization & Information Computing*, 16(1):849–877, 2026.

[84] C. M. Bishop. *Pattern Recognition and Machine Learning.* Springer, New York, NY, USA, 2006.

[85] C. Dwork. Differential privacy. In *Proceedings of the 33rd International Colloquium on Automata, Languages and Programming (ICALP)*, pages 1–12, Venice, Italy, 2006.

[86] I. Goodfellow, Y. Bengio, and A. Courville. *Deep Learning.* MIT Press, Cambridge, MA, USA, 2016.

[87] K. Pearson. Notes on regression and inheritance in the case of two parents. *Proceedings of the Royal Society of London*, 58:240–242, 1895.

[88] L. Wilkinson and M. Friendly. The history of the cluster heat map. *The American Statistician*, 63(2):179–184, 2009.

[89] E. R. Tufte. *The Visual Display of Quantitative Information.* Graphics Press, Cheshire, CT, USA, 2 edition, 2001.

[90] J. D. Hunter. Matplotlib: A 2d graphics environment. *Computing in Science & Engineering*, 9(3):90–95, 2007.